# Nanoscale Intermolecular Interactions between Human Serum Albumin and Alkanethiol Self-Assembled Monolayers

M. A. Rixman,[†] D. Dean,[‡] C. E. Macias,[†] and C. Ortiz*,[†]

*Department of Materials Science and Engineering, and Department of Electrical Engineering and Computer Science, Massachusetts Institute of Technology, RM 13-4022, 77 Massachusetts Avenue, Cambridge, Massachusetts 02139*

*Received September 13, 2002. In Final Form: January 13, 2003*

To study the molecular origins of hemocompatibility, the blood plasma protein human serum albumin (HSA) was covalently grafted to a nanosized probe tip at the end of a soft, microfabricated cantilever force transducer. The net force versus separation distance between the HSA-modified probe tip and three different model surfaces, including (1) gold; (2) a hydrophobic, $CH_3$-terminated alkanethiol self-assembling monolayer (SAM); and (3) a hydrophilic, $COO^-$-terminated alkanethiol SAM in aqueous sodium phosphate buffer solution (PBS, ionic strength (IS) = 0.01 M, pH = 7.4), was recorded and compared to the values of various theoretical models. The approach interaction of the HSA probe tip on the $COO^-$-terminated SAM and Au substrates was found to be purely repulsive for $D < 15$ nm, nonlinear with decreasing separation distance, and consistent with electrostatic double layer repulsion. The approach interaction of the HSA probe tip on the $CH_3$-terminated SAM substrate was found to be purely attractive, long range ($D < 80$ nm), nonlinear with decreasing separation distance, and much greater in magnitude and range than that known for van der Waals interactions between hydrocarbon SAMs terminated with hydrophilic chemical groups on Au. Large adhesive energies were observed for the HSA probe tip on both the $CH_3$-terminated SAM and Au surfaces ($\leq -29$ mN/m, $-22$ to $-73 k_B T$/protein), while smaller adhesive energies were observed on the $COO^-$-terminated SAM surface ($\leq -4.9$ mN/m, $-5.3$ to $-12 k_B T$/protein). It was shown that short-range adhesive contacts between the HSA chain segments and these surfaces give rise to energy dissipating mechanisms, such as HSA entropic molecular elasticity and enthalpic unfolding forces (deformation and rupture of noncovalent intramolecular bonds) and noncovalent bond rupture of the HSA chain segments adsorbed to the surface.

## Introduction

The interaction between the surface of an implanted artificial medical device and blood typically results in nonspecific, noncovalent surface adsorption of blood plasma proteins followed by platelet adhesion and activation, initiation of the coagulation cascade, and thrombus formation.[1,2] In the absence of transport limitations, the interaction potential between the protein and the surface as a function of separation distance, $U(D)$, will determine whether a protein will adsorb and at what rate. $U(D)$ is typically a superposition of numerous nonspecific repulsive (e.g. electrostatic counterion double layer, steric, hydration, etc.) and attractive (e.g. van der Waals, hydrophobic, H-bonding, ionic, etc.) components that can lead to complicated functional forms that vary with the strength and range of the constituent interactions.[3,4] Generally, improved protein resistance can be achieved by maximizing repulsive interactions and minimizing attractive ones. Subsequent stages of protein adsorption become increasingly complex and depend on the conformation, orientation, and mobility of the adsorbed proteins, the time-scale of conformational changes, protein exchange and desorption, and interactions of adsorbed proteins with each other.[5] The kinetics of the adsorption process and the time-dependent nature of the adsorbed biofilm (e.g. thickness, chemical structure, morphology, etc.) can be probed by a variety of experimental techniques such as radiolabeling, total internal refelection fluorescence, surface plasmon resonance, ellipsometry, optical waveguide light mode spectroscopy, attenuated total reflectance Fourier transform infrared spectroscopy, neutron and X-ray reflectivity, quartz crystal microbalance, electrical techniques, atomic force microscopy (AFM) imaging, and contact angle measurements. A variety of standards[6−9] also exist for in vitro hemocompatibility testing using biochemical and immunological assays to test for thrombosis, coagulation, platelet count, and so forth which are quicker and less costly than in vivo clinical trials. Although widely investigated and discussed in the literature, hemocompatibility, which varies greatly from material to material, is still poorly understood. Hence, attempts to prepare thromboresistant blood-contacting devices such as hemodialysis membranes, intra-arterial chemical sensors and catheters, vascular grafts, and blood pressure monitors have met with limited success.

To attack this problem, we have employed the powerful method of high-resolution force spectroscopy (HRFS) to directly measure the net nanoscale intermolecular force between a probe tip covalently bound with blood plasma proteins and a variety of model nonpolymeric planar surfaces as a function of protein−surface separation

* Corresponding author. E-mail: cortiz@mit.edu.
[†] Department of Materials Science and Engineering.
[‡] Department of Electrical Engineering and Computer Science.

(1) Lane, D. A.; Bowry, S. K. *Nephrol., Dial., Transplant.* **1993**, *9*, 18−28.
(2) Anderson, J. M.; Kottke-Merchant, K. *CRC Crit. Rev. Biocompat.* **1985**, *1*, 111−204.
(3) Halperin, A.; Leckband, D. *C. R. Acad. Sci. Paris: Polym. Interfaces* **2000**, *Ser. IV*, 1171−1178.
(4) Leckband, D. *Annu. Rev. Biophys. Biomol. Struct.* **2000**, *29*, 1−26.
(5) Ostuni, E.; Chapman, R. G.; Liang, M. N.; Meluleni, G.; Pier, G.; Ingber, D. E.; Whitesides, G. M. *Langmuir* **2001**, *17*, 6336−6343.
(6) *International Organization for Standardization, ISO 10993-4.*
(7) *European Standard, EN 30993.*
(8) *American Society for Testing and Materials, ASTM F-756.*
(9) *British Standard, BS 5736.*

10.1021/la026551f CCC: $25.00 
Published on Web 06/27/2003

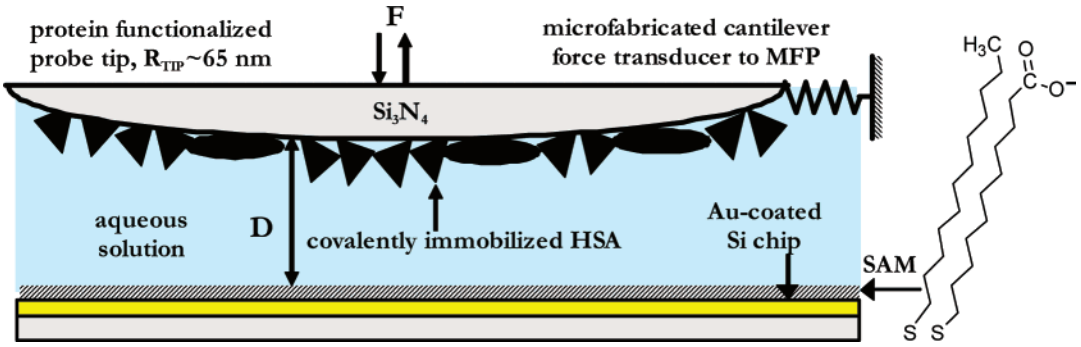


**Figure 1.** HRFS experimental setup.

distance, $F(D)$, where $U(D) = -\int F(D)\,dD$. As we describe in this paper, a more complete understanding of the molecular origins of the protein adsorption process can be achieved through deconvolution of the contributions of each of the individual constituent interactions. This goal can be realized through rigorous experimental and theoretical methodologies, by varying the environmental (solution) conditions and sample characteristics in conjunction with various theoretical model predictions using independently measured parameters. Although HRFS experiments yield an approximation of the actual potential experienced during the initial in vivo adsorption process (e.g. since the proteins are constrained in mobility on the probe tip, brought near the surface at a near-constant rate, and isolated from other blood components), experiments on synthetic polyelectrolytes have successfully correlated molecular level forces with adsorbed layer thicknesses measured via ellipsometry.[10] Given this fact, HRFS has great potential to be a useful tool for predicting adsorption kinetics,[11−14] evaluating and prescreening candidate biomaterials for which only extremely small quantities of material are available, and assisting in the chemical design of new hemocompatible biomaterials.

In the research presented here, human serum albumin (HSA) (the most abundant human blood plasma protein, and that which is typically the first to adsorb[15]) was covalently grafted to a nanosized silicon nitride ($Si_3N_4$) probe tip at the end of a soft, microfabricated cantilever force transducer. As shown in Figure 1, $F(D)$ was recorded between the HSA-modified probe tip and three different surfaces, including (1) gold, (2) a hydrophobic, $CH_3$-terminated alkanethiol self-assembling monolayer (SAM), and (3) a hydrophilic, $COO^-$-terminated alkanethiol SAM, both on "approach" (i.e. as the probe tip moves toward the surface) and "retract" (i.e. as the probe tip moves away from the surface) in aqueous sodium phosphate buffer solution (PBS, ionic strength (IS) = 0.01 M, pH = 7.4). SAMs are widely regarded as excellent model surfaces to study protein interactions due their highly uniform, crystalline-like structure, ease of varying chemical headgroup functionality, ease of deposition, and robustness.[16] A new nanomechanical instrument, the Molecular Force Probe (*Asylum Research*, Santa Barbara, CA), which has a limit of force detection = ±5 pN (for the specific cantilevers used in this study) and a limit of displacement detection = ±3 Å, was used to carry out the HRFS measurements. The approach data were analyzed through a comparison with molecular level theoretical models for the individual constituent components of the total net force (e.g. van der Waals,[17] electrostatic counterion double layer[18]), and the retract data were analyzed statistically using adhesive contact mechanical theories.[19−21] This study was critical to the interpretation and understanding of a series of parallel experiments conducted on more complex surfaces containing chemically end-grafted polymer chains,[22] a situation more commonly found in clinical applications.

## Experimental Methods

**High-Resolution Force Spectroscopy (HRFS) Measurements.** HRFS experiments were conducted using a new cantilever-based instrument, the Molecular Force Probe (MFP) (Asylum Research, Santa Barbara, CA) to measure force, $F$ (nN), versus tip−sample separation distance, $D$ (nm) (henceforth referred to and labeled on graphs as "Distance"), on approach and retract. A full description of this instrument, its limit of force and displacement detection in fluids, procedures for spring constant calibration and conversion of raw data, details of measurement errors, and a description of typical force versus distance curves, including the mechanical instabilities of the cantilever, are given in our previous works.[10,23] It should be noted that, in all HRFS experiments, the spring constant of the cantilever, $k_c$, is much less than the stiffness of the underlying (Au) substrate. Hence, little or no deformation of the substrate occurs, leading to the $D = 0$ vertical region of apparent infinite slope in the high-force, constant compliance regime, and all forces measured are surface forces rather than contact mechanical forces due to substrate elastic and/or plastic deformation. Force (nN) versus distance (nm) curves were measured at room temperature using a Thermomicroscopes microfabricated V-shaped $Si_3N_4$ cantilever ($k_c \sim 0.01$ N/m, cantilever length = 320 $\mu$m, resonance frequency = 850 Hz) with unsharpened square pyramidal probe tips at the end that had been modified with HSA as described in the following section. The HRFS experimental parameters for all experiments reported here included $z$-piezo range = 1 $\mu$m, rate of data acquisition = 5000 points/s, and constant $z$-piezo displacement rate = 1 $\mu$m/s (slow enough to minimize hydrodynamic effects), with the piezo reversing immediately between approach and retract cycles (no dwell time on the surface), and all experiments were conducted in phosphate buffer saline (PBS)

(10) Jiang, X.-P.; Ortiz, C.; Hammond, P. *Langmuir* **2002**, *18*, 1131−1143.
(11) Von Smoluchowski, M. *Z. Phys. Chem.* **1917**, *92*, 129−168.
(12) Kramers, H. A. *Physica* **1940**, *7*, 284.
(13) Hammes, G. G. *Principles of Chemical Kinetics*; Academic Press.: New York, 1978.
(14) van Oss, C. J. *J. Mol. Recognition* **1997**, *10* (5), 203−216.
(15) Vroman, L.; Adams, A. L. In *Proteins at Interfaces*; Brash, J. L., Horbett, T. A., Eds.; Washington, DC, 1987; pp 154−164.
(16) Schrieber, F. *Prog. Surf. Sci.* **2000**, *65*, 151−256.
(17) Derjaguin, B. V. *Kolloid Z.* **1934**, *69*, 155−164.
(18) Parsegian, V. A.; Gingell, D. *Biophys. J.* **1972**, *12*, 1192−1204.
(19) Derjaguin, B. V.; Muller, V. M.; Toporov, Y. P. *J. Colloid Interface Sci.* **1975**, *53*, 314−326.
(20) Burnham, N. A.; Colton, R. J. In *Scanning Tunneling Microscopy and Spectroscopy: Theory, Techniques, and Applications*; Bonnel, D. A., Ed.; VCH Publishers: New York, 1993; pp 191−249.
(21) Johnson, K. L.; Kendall, K.; Roberts, A. D. *Proc. R. Soc. London* **1971**, *A324*, 301−313.
(22) Rixman, M.; Dean, D.; Ortiz, C. *Langmuir*, submitted for publication.
(23) Seog, J.; Dean, D.; Grodzinsky, A.; Plaas, A.; Wong-Palms, S.; Ortiz, C. *Macromolecules* **2002**, *35*, 5601−5615.

solution (pH = 7.4, IS = 0.01 M). PBS solutions were made using sodium phosphate buffer tablets (Sigma lot #59H03371) which contain 8 g/L NaCl, 0.2 g/L $K^+H_2PO_4^-$, 1.15 g/L $2Na^+ \cdot HPO_4^{2-}$, and 0.2 g/L KCl. PBS stock solutions were diluted to obtain solutions with an IS = 0.01 M. Dilution did not have any effect on the efficacy of the buffer (i.e. the pH of the diluted buffer solutions remained stable). All water used for solutions, rinsing, and storage was first deionized (18 MΩ·cm resistivity, Purelab Plus UV/UF, US Filter, Lowell, MA) and then filtered through Millipore syringe filters (pore size = 0.22 $\mu$m) prior to use. The force versus distance curves on approach from at least three different sites on the sample surface were averaged (minimum of 50 curves per site), and the standard deviations were calculated and reported. Upon retraction, the full force versus distance curves were not averaged because of the large adhesion force and distance distributions inherent in the nonspecific adhesion events, which would smooth out many characteristic features of the curve. Rather, statistical analysis of the maximum forces and distances of adhesion under each of the experimental conditions was performed. The normalized $F/R_{tip}$ (mN/m) values (where $R_{tip}$ is the end radius of curvature of the probe tip measured by scanning electron microscopy) are reported along with the unnormalized $F$ (nN) on a double $y$-axis for all experimental data presented.

**Surface Preparation and Characterization.** Silicon (100) wafers (Recticon Enterprises, Inc., Pottstown, PA; test grade) were cleaned with ethanol and immediately coated with 2 nm of chromium to promote adhesion, followed by 100 nm of Au deposited using a thermal evaporator at 1.5 Å/s at room temperature at a pressure of $2 \times 10^{-6}$ Torr. These polycrystalline Au surfaces have a typical root-mean-square (rms) surface roughness of 2 nm and an Au island size range of 25−76 nm, as measured by contact mode atomic force microscopy (AFM) in air (taken with a Digital Instruments Multimode). The Au-coated Si wafers were cleaned using piranha solution (3:1 concentrated $H_2SO_4/H_2O_2$ (30%)) for 10 min just before further chemical modification and testing by MFP experiments. *[WARNING! Piranha solution is extremely oxidizing, reacts violently with organics, and should only be stored in loosely tightened containers to avoid buildup of pressure.]* Hydrophobic $CH_3$-terminated SAMs were prepared by incubating piranha-cleaned, 1 $cm^2$ gold substrates in dodecanethiol, $CH_3(CH_2)_{11}SH$ (Aldrich #47,136-4) (5 mM solution in ethanol), for 48 h, which was followed by rinsing with hexanes and subsequently PBS before experimentation. Hydrophilic COOH-terminated SAMs were prepared by incubating a piranha-cleaned, 1 $cm^2$ gold wafers in a 2 mM solution of 11-mercaptoundecanoic acid ($HS(CH_2)_{10}CO_2H$, Aldrich #45,056-1) in 100% ethanol for 48 h, followed immediately by rinsing with deionized (DI) water and then PBS before experimentation.[10] Advancing and receding surface contact angles ($\theta_{W(A)}$ and $\theta_{W(R)}$, respectively) were measured with DI water and found to be $\theta_{W(A)} = 111° \pm 1°$ and $\theta_{W(R)} = 108° \pm 2°$ for the $CH_3$-terminated SAM, $\theta_{W(A)} = 97° \pm 2°$ and $\theta_{W(R)} = 70° \pm 6°$ for the polycrystalline Au, and $\theta_{W(A)} = 44° \pm 1°$ and $\theta_{W(R)} = 13° \pm 1°$ for the $COO^-$-terminated SAM. Alkanethiol SAMs on Au(111) are known to have a $(\sqrt{3}\times\sqrt{3})$R30° structure relative to the underlying substrate, corresponding to a molecule−molecule spacing of ∼5 Å and an area per molecule of 21.6 $Å^2$ with an all-trans, planar zigzag hydrocarbon chain tilted by ∼34° from the surface normal, ∼1.5 nm in height.[16]

**Covalent Attachment of Human Serum Albumin on $Si_3N_4$ Cantilever Probe Tips.** 55 wt % of blood is plasma or serum (pH 7.4, IS = 0.15 M) which contains 6−8% proteins (over 3000 different types) including 58% albumins, 38% globulins, and 4% fibrinogens, most of which possess a net negative charge.[24] The model protein chosen for these studies is the highly water-soluble plasma protein human serum albumin (HSA), which is the smallest and most abundant plasma protein in the human body, accounting for 55% of the total protein in blood plasma. HSA is a single-stranded polypeptide whose amino acid sequence is known.[25] Its ionizable groups include 116 total acidic groups (98 carboxyl and 18 phenolic-OH) and 100 total basic groups (60 amino, 16 imidazolyl, 24 guanidyl). The absolute molecular weight of 66 436 g/mol was calculated from the numbers and molar masses of the constituent amino acid residues, which yields a contour length of the denatured protein of $L_{contour}$(HSA) = 216 nm (as calculated from the number of residues and a peptide bond length of 0.37 nm). HSA contains 17 disulfide bridges, one free thiol (Cys 34), and a single tryptophan (Trp 214). HSA typically binds 1−2 fatty acids per protein,[26] which effectively reduces the isoelectric point (pI, i.e., the pH at which the total charge including bound ions is zero); in 0.15 M NaCl the pI for lipid-bound HSA is 4.7,[27] while pI = 5.7 for defatted HSA.[28] At pH 7.4, the shape of native HSA in solution is thought to be a prolate ellipsoid of revolution with major and minor axes, respectively, 12.0 and 2.7 nm,[29] or 14.1 and 4.1 nm,[30,31] linking three homologous, globular domains in series, each carrying net charges of −9$e$ (domain I, N-terminal), −8$e$ (domain II), and +2$e$ (domain III, C-terminal), giving a total net charge for the protein of −15$e$ (calculated from the amino acid composition)[26] or −19$e$ measured experimentally (due to additional bound ions) at pH 7.4 (the pH of blood)[32] (Figure 2; adapted from ref 33). X-ray determinations of the structure of HSA in a crystal have suggested a "heart-shaped" structure, also with three homologous domains, which can be represented by an equilateral triangle with sides of approximately 8 nm each and an average thickness of 3 nm (Figure 3).[34−36] HSA is a dynamic, rapidly moving, "breathing" molecule having a rotational diffusion coefficient of ∼20 ns[26]), and it is known to have some degree of flexibility, expansion, and contraction, which enables significant conformational transitions; hence, the average shape that HSA takes on in aqueous solution is unclear.[37,38] It is believed that there are six helical subdomains which form hydrophobic channels with basic and hydrophobic amino acid residues placed at the ends, while the overall surface remains extremely hydrophilic (Figure 3D; hydrophilic residues are colored blue and hydrophobic residues are green). As determined from X-ray diffraction, HSA is 67% α-helical, with the remainder in $\beta$-turns and extended polypeptide chains, and contains no $\beta$-sheet structure.[26] HSA is known to have a 0.55 nm thick monolayer of closely associated water molecules on its surface, with most (98%) oriented with their H atoms pointed toward the protein surface. The next layer of water is about 30% oriented, creating a "fuzzy" hydrated interphase in aqueous solution.[26]

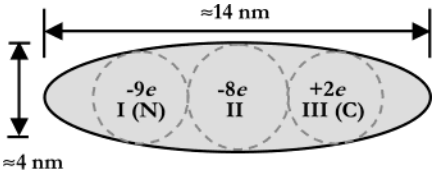


**Figure 2.** Schematic of proposed HSA ellipsoidal shape in solution, showing the dimensions and net charges of its three domains.[33]

HSA was covalently attached to $Si_3N_4$ cantilever probe tips using the chemical reaction scheme shown in Figure 4.[39,40] Aminobutyldimethylmethoxysilane (ABDMS, #S565350), glut-

(24) Blombaek, B.; Hanson, L. *Plasma Proteins*; John Wiley & Sons: New York, 1979.
(25) Dayhoff, M. O. *Atlas of Protein Sequence and Structure*; National Biomedical Foundation: Washington, DC, 1972.
(26) Peters, T. *All About Albumin: Biochemistry, Genetics, and Medical Applications*; Academic Press: New York, 1992.
(27) Longsworth, L. G.; Jacobsen, C. F. *J. Phys. Colloid. Chem.* **1949**, *53*, 126.
(28) Gianazza, E.; Firgerio, A.; Astrua-Testori, S.; Righetti, P. G. *Electrophoresis* **1984**, *5*, 310.
(29) Haynes, C. A.; Norde, W. *Colloids Surf., B: Biointerfaces* **1994**, *2*, 517.
(30) Peters, T. *Adv. Protein Chem.* **1985**, *37*, 161.
(31) Soderquist, M. E.; Walton, A. G. *J. Colloid. Interface Sci.* **1980**, *75*, 386.
(32) Tanford, C. *J. Am. Chem. Soc.* **1950**, *72*, 441.
(33) Ladam, G.; Gergely, C.; Senger, B.; Decher, G.; Voegel, J.-C.; Schaaf, P.; Cuisinier, F. J. G. *Biomacromolecules* **2000**, *1*, 674.
(34) Curry, S.; Mandelkow, H.; Brick, P.; Franks, N. *Brookhaven Protein Databank*: http://www.rcsb.org/pdb.
(35) Curry, S.; Mandelkow, H.; Brick, P.; Franks, N. *Nat. Struct. Bio.* **1998**, *5*, 127.
(36) Carter, D. C.; Ho, J. X. *Adv. Protein Chem.* **1994**, *45*, 153−204.
(37) Blomberg, E.; Claesson, P. M.; Tilton, R. D. *J. Colloid Interface Sci.* **1994**, *166*, 427.
(38) Kragh-Hansen, U. *Pharmacol. Rev.* **1981**, *33*, 17.

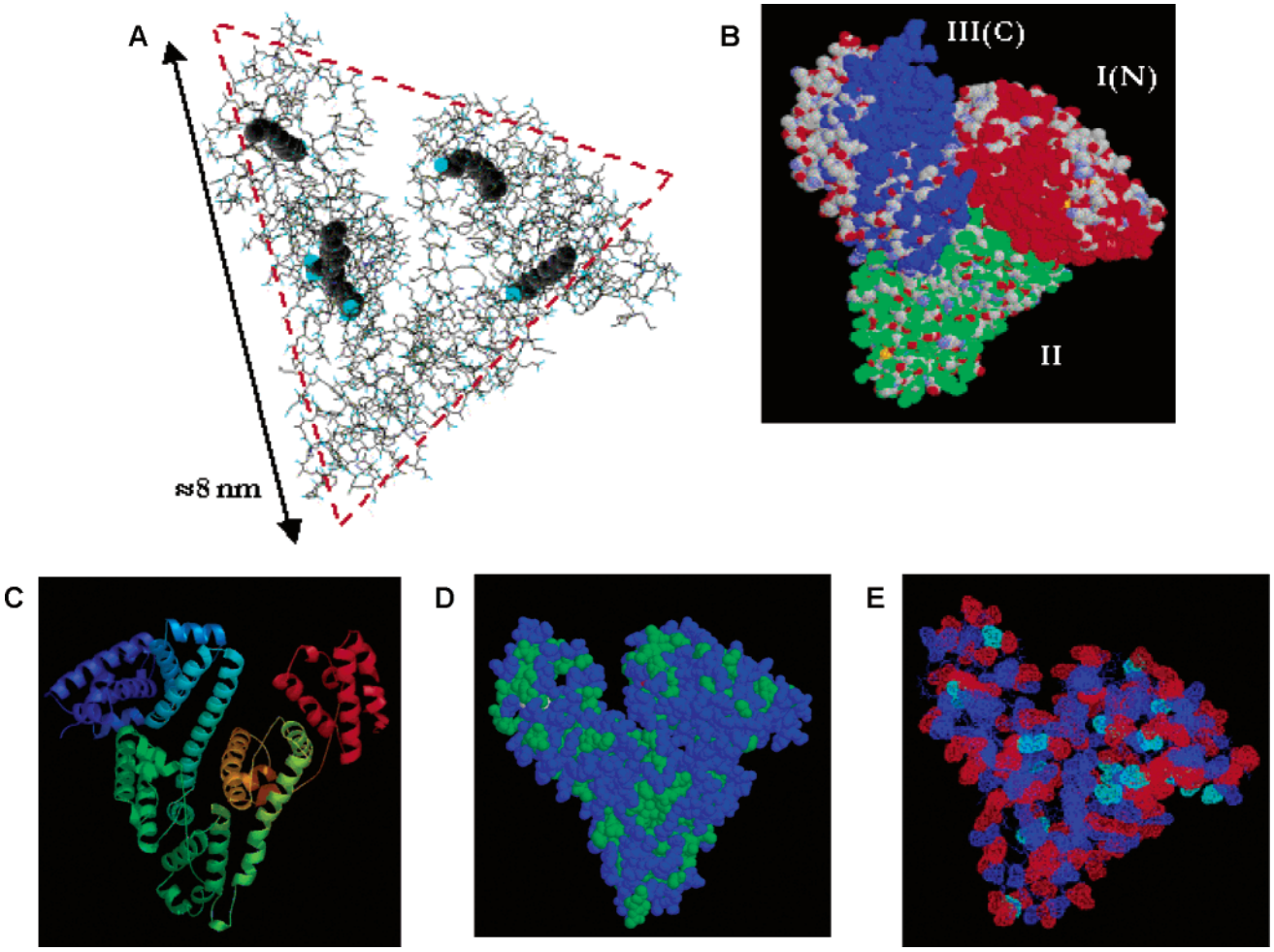


**Figure 3.** Various schematics of a crystallized HSA complexed with myristic acid (downloaded from ref 34; also see ref 35). Part A is a wireframe display showing the dimensions of HSA and binding sites for complexed fatty acids. In the crystalline form HSA approximates an 8 nm-sided equilateral triangle ~ 3 nm deep. Parts B and C depict space-filling and ribbon models marking the three domains I, II, and III, labeled in red, green, and blue, respectively. Part D is a space-filling display showing the locations of hydrophilic residues (colored blue) and hydrophobic residues (in green). Part E is a wire frame backbone display with charged residues using a van der Waals dotted surface. All lysines and arginines (both positively charged at pH 7) are colored blue, aspartic acid and glutamic acid (negatively charged at pH 7) are colored red, and histidine, which is 90% negatively charged at pH = 7, is in cyan.

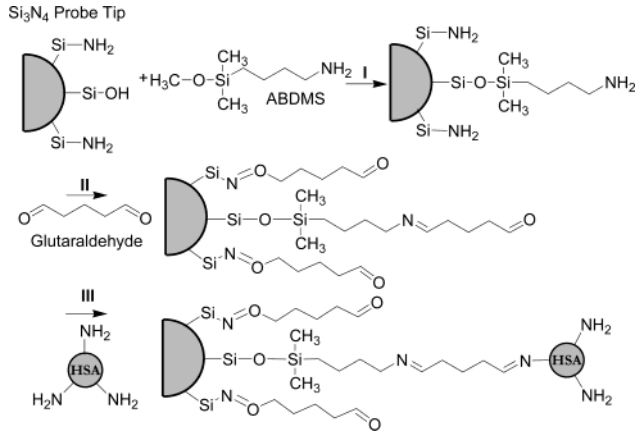


**Figure 4.** Reaction scheme for the covalent attachment of HSA to a $Si_3N_4$ probe tip. HSA may form multiple tethers to the probe tip via any of its 60 free amino groups.

araldehyde (#G-8552, lot #31K5306), and HSA (#A9511, lot #126H9322, containing bound fatty acids) were purchased from Sigma. These $Si_3N_4$ probe tips were prepared by chemical vapor deposition using a 4:1 mixture of dichlorosilane and ammonia gases, respectively, resulting in approximately a 4:1 ratio of SiOH/$SiNH_3$ surface groups.[41] $Si_3N_4$ probe tips were cleaned and oxidized in an oxygen plasma for 10 s at 30 Pa and 10 W power immediately prior to modification. They were then immersed in a 4% (v/v) toluene solution of ABDMS for 2 h. The silanized probes were rinsed in methanol followed by 0.01 M PBS before being immersed in a 2.5% (v/v) aqueous solution of glutaraldehyde for 30 min and then rinsed with an excess of DI water. The cantilevers and probe tips were then incubated in a 0.01% (w/v) HSA solution (in 0.01 M PBS) for 1 min. Finally, the HSA-modified probe tips were rinsed copiously with PBS and stored in the same concentration buffer until tested. The ABDMS and glutaraldehyde molecules provide a short linker for the HSA off the probe tip which may allow for some flexibility and retention of the native movements of the protein. Multiple covalent linkages are possible, and it should be noted that the exact orientation and conformation of the HSA on the probe tip are not known.

**Characterization of Human Serum Albumin Covalent Attachment Reaction.** The success and optimization of the HSA chemical grafting reaction to form a monolayer on the probe tip was a critically important component of this work and was verified by three different methodologies. Data obtained by all

(39) Vinckier, A.; Heyvaert, I.; D'Hoore, A.; McKittrick, T.; Van Haesendonck, C.; Engelborghs, Y.; Hellemans, I. *Ultramicroscopy* **1995**, *57*, 337.

(40) Vansteenkiste, S. O.; Corneillie, S. I.; Schacht, E. H.; Chen, X.; Davies, M. C.; Moens, M.; Van Vaeck, L. *Langmuir* **2000**, *16*, 3330.

(41) Ruiter, T. Personal communication, 2002.

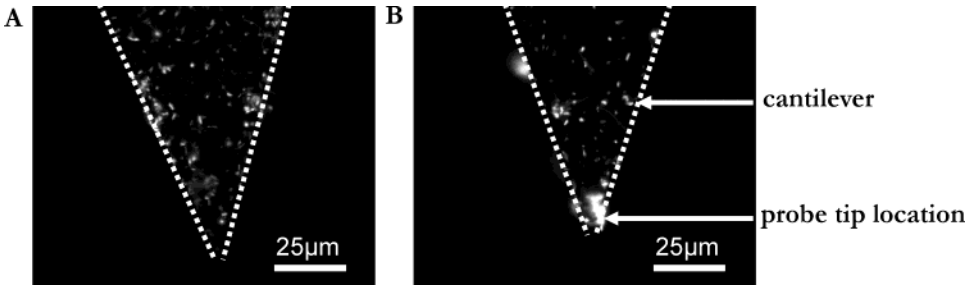


**Figure 5.** Fluorescence microscope image of (A) the glutaraldehyde control cantilever and (B) an HSA-modified cantilever. White dashed lines are included to guide the eye to the outline of the cantilever.

three approaches were compared to those for control samples which involved the same chemical procedure as was used in the probe tip modification, in which the final reaction step in the chemical procedure was carried out in HSA-free buffer rather than 0.01% (w/v) HSA (henceforth referred to as "glutaraldehyde control").

*(A) Contact Angle Measurements and AFM Imaging.* Characterization of HSA grafted to planar $Si_3N_4$ wafers (prepared by chemical vapor deposition at 780 °C and 0.25 Torr of a 10:1 mixture of dichlorosilane and ammonia gases, respectively, thus resulting in approximately a 10:1 ratio of $SiOH/SiNH_3$ surface groups) was carried out by contact angle measurements and contact mode AFM imaging in PBS (Digital Instruments Multimode). Planar $Si_3N_4$ wafers needed to be employed for these standard techniques, since they are not able to measure on the small surface area of the probe tips. Advancing contact angles were 44 ± 1° for the HSA surface and 62.9 ± 5.8° for the glutaraldehyde control. AFM imaging of the HSA-grafted surface suggested complete coverage of the surface with the HSA and showed rounded features 10 nm in relative height that were not observed on the glutaraldehyde control, which showed jagged features approximately 5 nm in relative height.

*(B) Fluorescence Microscopy.* Second, glutaraldehyde and HSA-functionalized cantilevers and probe tips were tagged with a fluorescent compound by immersing for 48 h in a solution of 1.0 mL of 0.01 M PBS and 0.25 mL of a $6.67 \times 10^{-4}$ M solution of Oregon Green Dye (Molecular Probes Product # O-6147) in dimethyl sulfoxide (DMSO). In this procedure, an active ester on the fluorescent dye readily covalently reacts with free amine groups on the protein but not with aldehyde groups on the glutaraldehyde "control." The cantilevers were then rinsed thoroughly first with DMSO and then with 0.01 M PBS, and finally stored in PBS until viewing with the fluorescence microscope (Zeiss Axiovert 200 fluorescence microscope equipped with a Xe lamp using a 40× objective lens). Excitation was set at a wavelength of 488 nm, emission was detected in the range 510−520 nm, and the two chips were imaged in the same sample well so that background fluorescence could be subtracted from the final images. Total exposure time was 10 ms, and data collection was done by *z*-sampling every 1 $\mu$m for a total depth of 60 $\mu$m. The images were taken using a 40× oil-immersion objective collecting on a cool-snap HQ OCD camera. After the images were collected, the background fluorescence was subtracted and the relative brightness was scaled identically for both images, so that the two could be directly compared. Although some nonspecific adsorption of the Oregon Green inevitably occurred on both substrates due to poor solubility of the compound in water, fluorescence on the HSA-grafted cantilever (Figure 5B) was found to be 8.2 times more intense than that on the glutaraldehyde control (Figure 5A). It should be noted that the probe tip, located at the end of the cantilever, is not visible under such low magnification.

*(C) HRFS.* Last, HRFS experiments in PBS were employed to optimize the grafting reaction conditions to produce a well-packed HSA monolayer (as opposed to adsorbed multilayers). The HSA-modified probe tip versus a hydrophobic control surface ($CH_3$-terminated SAM) showed the presence of long-range, nonlinear attractive forces due to the stretching (unfolding) of protein chains between the probe tip and adsorbed segments which tether the protein to the hydrophobic surface. For the probe tip reaction conditions employed, the distance ranges of these long-range protein unfolding events were almost always less than the calculated contour length of an individual HSA molecule, suggesting a monolayer on the probe tip surface. For longer reaction times in step III (of Figure 4), the unfolding lengths were observed at distances up to many times greater than the contour length, suggesting multiple adsorbed layers. In addition, the glutaraldehyde control probe tip tested via HRFS showed distinctly different force spectroscopy behavior in magnitude, range, and shape compared to the case of the HSA probe tip on a variety of surfaces tested (data not shown).

**Table 1**

| | $CH_3$ SAM | $COO^-$ SAM | Au |
|---|---|---|---|
| $D_{max}$ (nm) | 80 | 15 | 15 |
| $R_{tip}$ (nm) | 65 | 150 | 65 |
| HSA $A_{tip}$ (nm$^2$) at $D = 0$ | 16 000 | 7100 | 3100 |
| $A_{triangle}$(HSA) (nm$^2$) | 28 | 28 | 28 |
| $A_{ellipse}$(HSA) (nm$^2$) | 45 | 45 | 45 |
| $A_{substrate}$ (nm$^2$) at $D = 0$ | 12 000 | 13 000 | 5500 |
| no. of proteins in $A_{tip}$ at $D = 0$[a] | 580 | 260 | 110 |
| no. of proteins in $A_{tip}$ at $D = 0$[b] | 350 | 160 | 68 |
| $A_{SAM\ molecule}$ (nm$^2$) (ref 16) | 0.216 | 0.216 | 0.216 |
| no. of SAM molecules in $A_{substrate}$ | 56 000 | 60 000 | |
| $F_{max}$ (nN) | 3.0 | 3.0 | 3.0 |
| $F_{max}$/protein[a] (pN) | 5.2 | 12 | 27 |
| $F_{max}$/protein[b] (pN) | 8.6 | 19 | 44 |
| $A_{contact}$ (nm$^2$) | 5.7 | 9.6 | 5.5 |
| no. of SAM molecules in $A_{contact}$ at $D = 0$ | 26 | 44 | |

[a] Assuming a triangularly shaped protein. [b] Assuming an elliptically shaped protein.

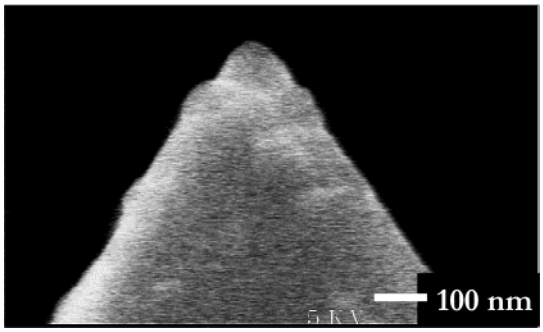


**Figure 6.** SEM image of an HSA-modified $Si_3N_4$ probe tip.

**Measurement of Probe Tip End Radii of Curvature (Table 1).** The radii of the chemically modified probe tips were determined for each individual cantilever by scanning electron microscopy (SEM) (JEOL 6320FV field-emission high-resolution SEM, operating voltage = 5 kV, magnitude = 100000×) (Figure 6), where $R_{tip}$ was determined by drawing two intersecting straight lines tangential to the sides of the probe tip and then drawing a circle tangential to both of them. $R_{tip}$ for the $COO^-$-terminated SAM probe tip was found to be ∼63 nm. $R_{tip}$ for the HSA probe tip used on the $COO^-$-terminated SAM surface was found to be ∼150 nm. $R_{tip}$ for the HSA probe tip used on the $CH_3$-terminated SAM and Au surfaces was found to be ∼65 nm.

**Probe Tip and Substrate Surface Interaction Areas.** The relevant areas for the force profiles *on approach* are the *surface interaction area of the probe tip and substrate.* The maximum probe tip and substrate surface interaction areas at $D = 0$, $A_{tip}$

and $A_{substrate}$, were approximated as shown in Appendix I for each probe tip−substrate combination from $R_{tip}$ and the maximum separation distance of interaction measured by HRFS on approach, $D_{max}$, and they were found to range from ∼3100 to 16 000 nm$^2$ and from 5500 to 13 000 nm$^2$, respectively. From these values, the maximum number of proteins, assuming a dense monolayer, in $A_{tip}$ (at $D = 0$) was calculated assuming either a triangular or ellipsoidal shape (lying flat) and found to range from 68 to 580 proteins. For a maximum applied force of $F_{max} =$ 3 nN at $D = 0$, the maximum force per protein was calculated and found to be <8.6 pN for a $CH_3$-terminated SAM, <19 pN for a $COO^-$-terminated SAM, and <44 pN for Au, much less than the expected force needed for mechanical denaturation.[42] Hence, it is expected that steric deformations of the protein on approach within the surface interaction area have a negligible contribution to the interaction force profile. Since the area per SAM molecule on the substrate is 0.216 nm$^2$,[16] the number of SAM molecules in $A_{substrate}$ was 56 000 for the $CH_3$-terminated SAM and 60 000 for the $COO^-$-terminated SAM.

**Probe Tip Contact Area.** On retract and relevant to adhesion data, in addition to the surface interaction area, there is a much smaller *elastic contact area* where the molecules on the probe tip apex and the molecules just under the probe tip apex on the substrate are in intimate contact. Within this small region, the forces are amplified, for example by 1.5 times the externally applied force, $F$, for Hertzian mechanics. The maximum elastic contact area, $A_{contact}$, was calculated from Hertzian elastic contact mechanics[43] for the substrates displaying no adhesive forces on approach (Appendix II) and was found to be 9.6 nm$^2$ for the $COO^-$-terminated SAM surface (corresponding to ∼44 SAM molecules) and 5.5 nm$^2$ for the Au surface. $A_{contact}$ was calculated from (modified Hertzian) Derjaguin−Muller−Toporov (DMT) theory[19] for the $CH_3$-terminated SAM displaying an adhesive jump-to-contact on approach and was found to be 5.7 nm$^2$ (corresponding to ∼26 SAM molecules). Hence, $A_{contact} \ll A_{substrate}$, $A_{tip}$, and $A_{protein}$; that is, much less than a single protein could fit in the maximum elastic contact area.

## Results and Discussion

**Interaction of HSA-Modified Probe Tip with Various Surfaces on Approach.** *(A) Control Experiment: $COO^-$-Terminated SAM Probe Tip versus $COO^-$-Terminated SAM Surface.* Figure 7 displays the average $F/R_{tip}$ (mN/m) and $F$ (nN) versus $D$ (nm) approach curves (with standard deviations) for a $COO^-$-terminated SAM probe tip versus a $COO^-$-terminated SAM surface in PBS,[10] compared to the case of Derjaguin−Landau−Verwey−Overbeek (DLVO) theory.[44,45] Under these solution conditions the carboxylic acid group is ionized and negatively charged (p$K_a = 5.5 \pm 0.5$).[46] Nonlinear, purely repulsive forces were observed for $D$ < 15 nm, reaching a maximum magnitude at $D = 0$ (upon reaching the constant compliance regime) of $F = 0.6$ nN, corresponding to a $F/R_{tip} \sim 10$ mN/m. Following the DLVO theory, the total interaction force was assumed to be a linear summation of an attractive van der Waals component and a repulsive electrostatic counterion double layer component:

$$F_{tot}(D) = F_{VDW}(D) + F_{electr}(D) \quad (1)$$

$F_{electr}(D)$ was modeled using a constant surface charge approximation based on the numerical solution to the nonlinear Poisson−Boltzmann (PB) equation including divalent ions in which the substrate is assumed to be a plane of constant charge per unit area ($\sigma_{plane}$) and the probe tip is modeled as an impermeable hemisphere of radius $R_{hemis}$, also with constant charge per unit area ($\sigma_{tip} \approx \sigma_{plane}$).[23,47,48] The force was obtained from the electrostatic potential, $\Phi$, using the so-called free energy method[47,49,50] and surface element integration (SEI).[51] In the theoretical data fits, the electrical interaction Debye length, $\kappa^{-1}$, was set to its known value for IS = 0.01 M ($\kappa^{-1} = 2.96$ nm), $R_{hemis}$ was fixed to the known value of $R_{tip}$ measured by SEM (≈63 nm), and $\sigma_{tip} \approx \sigma_{plane}$ was the single fitting parameter.

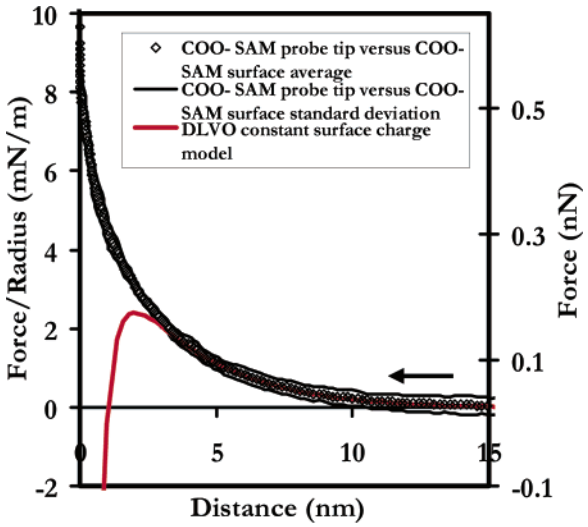


**Figure 7.** Average force (nN) and force/radius (mN/m) versus distance, $D$ (nm), approach curves for a $COO^-$-terminated probe tip versus a $COO^-$-terminated SAM surface in PBS (black diamonds) with standard deviations (black lines) compared to the DLVO electrostatic double layer constant surface charge model (red line). $\kappa^{-1} = 2.96$ nm (IS = 0.01 M), $A = 6.92 \times 10^{-20}$ J, and $R_{tip} = 63$ nm were fixed to their known values, and the charge per unit area was used as the only fitting parameter and found to be $\sigma_{tip}(COO^-) = \sigma_{plane}(COO^-) = -0.0178$ C/m$^2$.

The nonretarded van der Waals force was also included using the inverse square power law derived using the "Derjaguin approximation" (valid for $R \gg D$):[17]

$$F_{VDW}(D) = -\frac{AR}{6D^2} \quad (2)$$

where $F_{VDW}$ is the van der Waals force between a sphere of radius $R$ (assumed to be equal to the probe tip radius, $R_{tip}$) and a planar surface separated by a distance $D$, and $A$ is the nonretarded Hamaker constant, which was fixed. The Hamaker constant employed for the van der Waals component of the force for this system (Si/Cr/Au/HS$(CH_2)_{10}$-$CO_2^-$/aqueous electrolyte (IS = 0.01 M, pH = 7.4)/HS-$(CH_2)_{10}CO_2^-$/Au/Cr/$Si_3N_4$) was fixed to $A = 6.92 \times 10^{-20}$ J. This value was chosen on the basis of an average of fits of eq 2 to HRFS experimental results reported by us and others for similar hydrophilic-terminated SAM hemispherical probe tip−planar surface systems including $A = 5.2 \times 10^{-20}$ J for Si/Cr/Au/HS$(CH_2)_2SO_3^-$/aqueous electrolyte (IS = 0.1 M, pH = 5.6)/HS$(CH_2)_2SO_3^-$/Au/Cr/

(42) Rief, M.; Gautel, M.; Oesterhelt, F.; Fernandez, J. M.; Gaub, H. E. *Science* **1997**, *276*, 1109−1112.
(43) Hertz, H. *Hertz's Miscillaneous Papers*; MacMillan: London, 1896.
(44) Verwey, E.; Overbeek, W. J. T. *Theory of Stability of Lyophobic Colloids*; Elsevier: Amsterdam, The Netherlands, 1948.
(45) Derjaguin, B. V.; Landau, L. D. *Acta Physiochim. URSS* **1941**, *14*, 633.
(46) Vezenov, D. V.; Noy, A.; Rozsnyai, L. F.; Lieber, C. M. *J. Am. Chem. Soc.* **1997**, *119*, 2006−2015.
(47) Dean, D.; Seog, J.; Ortiz, C.; Grodzinsky, A. *Langmuir*, accepted for publication.
(48) Ninham, M.; Parsegian, A. *J. Theor. Biol.* **1971**, *31*, 405−428.
(49) Sharp, K. A.; Honig, B. *J. Phys. Chem. B* **1990**, *94*, 7684−7692.
(50) Jin, M.; Grodzinsky, A. J. *Macromolecules* **2001**, *34*, 8330−8339.
(51) Bhattacharjee, S.; Elimelech, M. J. *Colloid Interface Sci.* **1997**, *193*, 273−285.

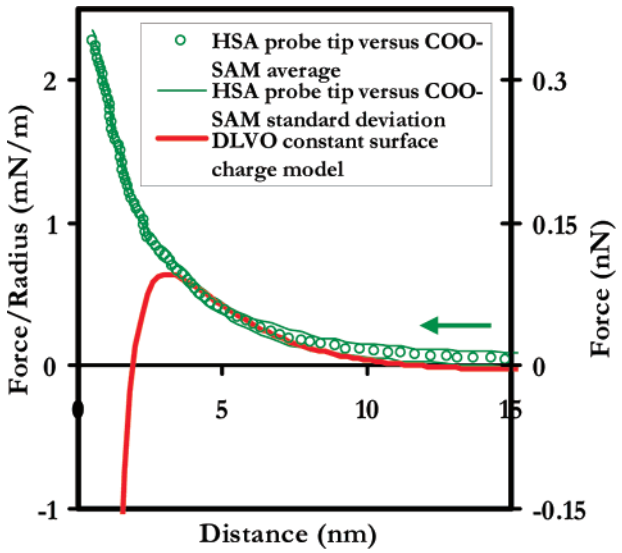


**Figure 8.** Average force (nN) and force/radius (mN/m) versus distance, $D$ (nm), approach curves for an HSA probe tip versus a $COO^-$-terminated SAM surface in PBS (green circles) with standard deviations (green lines) compared to the DLVO electrostatic double layer constant surface charge model (red line). $\kappa^{-1} = 2.96$ nm (IS = 0.01 M), $A = 6.92 \times 10^{-20}$ J, $\sigma_{plane}(COO^-) = -0.0178$ C/m$^2$, and $R_{tip} = 150$ nm were fixed to their known values, and the charge per unit area of the probe tip was used as the only fitting parameter and found to be $\sigma_{tip}(HSA) = -0.0064$ C/m$^2$.

$Si_3N_4$,[23] $A = 3.4 \times 10^{-20}$ J for glass/Ti/Au/$C_{16}$OH/HOH/$C_{16}$OH/Au/Ti/$Si_3N_4$,[52] $A = 10 \times 10^{-20}$ J for mica/Au/$C_{11}$OH/HOH/$C_{11}$OH/Cr/Au/SmCo,[53] $A = 12 \times 10^{-20}$ J for mica/Au/$C_{16}$OH/HOH/$C_{16}$OH/Cr/Au/SmCo,[53] and $A = 4 \times 10^{-20}$ J for Au/Cr/Au/HS$(CH_2)_{10}CO_2^-$/aqueous electrolyte (IS = 0.0001 M, pH = 4−6)/HS$(CH_2)_{10}CO_2^-$/Au/Cr/$Si_3N_4$.[54] As described in ref 52, the calculation of $A$ for our nine-layer systems could be performed using a Lifshitz multilayered model, but due to the lack of the ability to include conductors rigorously in such calculations, we have instead employed an average of experimental values reported on similar systems via HRFS, which will give a more accurate estimate of the magnitude, range, and functional form of the attractive van der Waals force.

DLVO theoretical data fits yielded a surface and probe tip charge per unit area, $\sigma_{plane}(COO^-) = \sigma_{tip}(COO^-)$, of −0.018 C/m$^2$. Allowing more than one free fitting parameter resulted in multiple solutions. The DLVO model fit the experimental data extremely well for $D > 3.4$ nm and increasingly deviated from the data with decreasing separation distance for $D < 3.4$ nm, possibly due to the assumption of uniform permittivity and the approximation of ions as discrete point charges in the electrostatic double layer model, which starts to break down at small distances, in addition to the presence of non-DLVO forces. No jump-to-contact minimum was observed, most likely due to the presence of additional non-DLVO forces, such as possible hydration repulsion at shorter distances. Such phenomena have been observed previously for hydrophilic SAMs and attributed to the additional energy needed to dehydrate surface adsorbed counterions.[23]

*(B) HSA Probe Tip versus $COO^-$-Terminated SAM Surface.* Figure 8 (green circles) shows the average $F$ (nN) and $F/R_{tip}$ (mN/m) versus $D$ (nm) approach curves (with standard deviations) for an HSA probe tip versus a $COO^-$-terminated SAM surface in PBS compared to the case of the DLVO constant surface charge model. Under these solution conditions, both the SAM and HSA have a net negative charge (pI(HSA) = 4.7 for lipid-bound HSA[27]). Similar to the data for the $COO^-$-terminated SAM probe tip versus $COO^-$-terminated SAM surface, nonlinear, purely repulsive electrostatic forces were observed to begin at $D < 15$ nm, reaching a maximum magnitude at $D = 0$ (upon reaching the constant compliance regime) of $F = 0.34$ nN, corresponding to a $F/R_{tip} \sim 2.3$ mN/m with no jump-to-contact observed. As before, the model parameters for this experiment (Si/Cr/Au/HS$(CH_2)_{10}CO_2^-$/aqueous electrolyte (IS = 0.01 M, pH = 7.4)/HSA/$Si_3N_4$) that were fixed in the simulation were the electrical interaction Debye length, $\kappa^{-1} = 2.96$ nm for IS = 0.01 M, $A = 6.92 \times 10^{-20}$ J,[55] $R_{tip} = 150$ nm, and $\sigma_{plane}(COO^-) = -0.018$ C/m$^2$ (taken from the DLVO theoretical data fits to the $COO^-$-terminated SAM probe tip versus $COO^-$-terminated SAM surface experiment described above). The surface charge model fit the experimental data well for $D > 3.8$ nm using one free fitting parameter, $\sigma_{tip}$(HSA), which was found to be equal to −0.0064 C/m$^2$. This value represents an average charge per unit area in the planes parallel to the outer exposed atomic van der Waals surface of the protein layer (which was taken to be the plane of constant charge in the model). Surface charge densities obtained in this manner via HRFS have been shown to accurately represent the spatial distribution of charged groups on the exposed protein surface when the protein is oriented uniformly (e.g. in a crystal) when compared to theoretical predictions of the electrostatic potential distribution around the protein surfaces calculated using the Poisson−Boltzmann equation.[56] In our experiment, however, there is no need to believe that the HSA layer on the probe tip is uniformly oriented, since the distribution of hydrophobic and hydrophilic sites and the distribution of amine groups through which the covalent attachment takes place are nonuniform (Figure 3D and E). Hence, the measured charge per unit area should reflect an average of the entire HSA surface charge distribution map (Figure 3E) and corresponds to a charge per protein of −1.8$e$ assuming an elliptical shape and −1.1$e$ assuming a triangular shape. The net charge of HSA under the experimental conditions employed here is known to be −15$e$, which takes into account the full amino acid sequence,[26] or −19$e$ measured experimentally at pH = 7.4 (including bound ions).[32] As expected, these values are greater than that obtained via HRFS, presumably because many of the charged groups may be unexposed, being located interior to the protein or underneath (facing the probe tip side).

*(C) HSA Probe Tip versus Au Surface.* Figure 9 (red squares) displays average $F$ (nN) and $F/R_{tip}$ (mN/m) versus $D$ (nm) approach curves (with standard deviations) for an HSA probe tip versus an Au planar surface in PBS compared to the DLVO constant surface charge model (black line). Similar to the data shown in Figures 7 and 8, a nonlinear, purely repulsive force was observed to begin at $D < 15$ nm, reaching a maximum magnitude at $D = 0$ (upon reaching the constant compliance regime) of $F = 0.32$ nN, corresponding to a $F/R_{tip} \sim 4.9$ mN/m with no jump-to-contact. The model parameters for this experiment (Si/Cr/Au/aqueous electrolyte (IS = 0.01 M, pH =

(52) Ederth, T.; Claesson, P.; Liedberg, C. *Langmuir* **1998**, *14*, 4782.
(53) Ashby, P. D.; Chen, L.; Lieber, C. M. *J. Am. Chem. Soc.* **2000**, *122*, 9467.
(54) Kane, V.; Mulvaney, P. *Langmuir* **1998**, *14*, 3303−3311.
(55) The Hamaker constant for the HSA versus $COO^-$ system may be somewhat lower than that for $COO^-$ versus $COO^-$ due to the presence of the thicker low dielectric protein layer on the probe tip, which would result in a slight overestimation of the fit HSA probe tip charge per unit area.
(56) Sivasankar, S.; Subramaniam, S.; Leckband, D.; Biophysics, P. U. V. p. O. *Proc. Natl. Acad. Sci. U.S.A.* 1998, 12961.

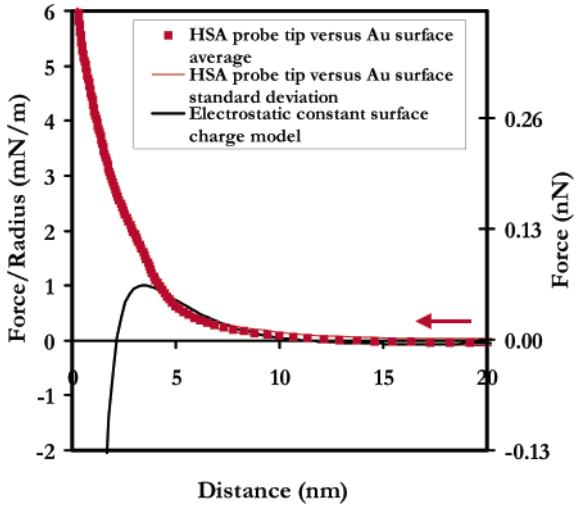


**Figure 9.** Average force (nN) and force/radius (mN/m) versus distance, $D$ (nm), approach curve for an HSA probe tip on a Au surface in PBS (red squares) with standard deviations (red lines). Comparison is made to DLVO theory (black line) fixing $\sigma_{tip}$(HSA) = −0.0064 C/m$^2$, $\kappa^{-1}$ = 2.96 nm (IS = 0.01 M), $R_{tip}$ = 65 nm, and $A = 6.92 \times 10^{-20}$ J. $\sigma_{plane}$(Au) was the only fitting parameter and was found to be 0.0144 C/m$^2$.

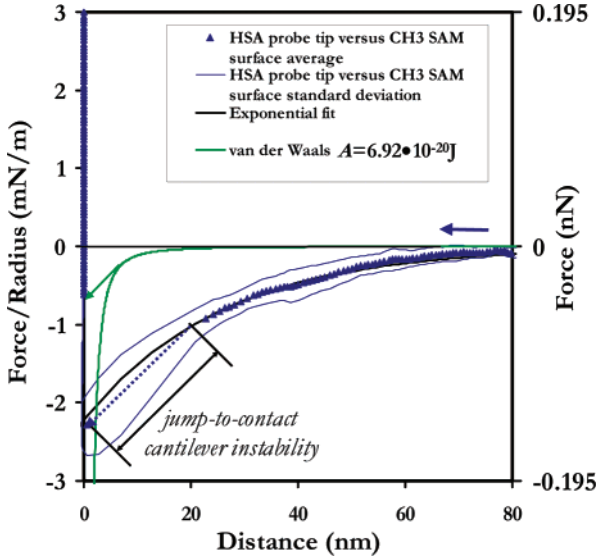


**Figure 10.** Average force (nN) and force/radius (mN/m) versus distance, $D$ (nm), approach curve for an HSA probe tip on a $CH_3$-terminated SAM surface in PBS (blue triangles) with standard deviations (blue lines). $R_{tip}$ = 65 nm. Comparison is made to the van der Waals force ($A = 6.92 \times 10^{-20}$ J) (green line) as well as to an exponential fit (black line).[61]

7.4)/HSA/$Si_3N_4$) that were fixed in the simulation were $\kappa^{-1}$ = 3 nm for IS = 0.01 M, $A = 6.92 \times 10^{-20}$ J, $R_{tip}$ = 65 nm, and $\sigma_{tip}$(HSA) = −0.0064 C/m$^2$ (taken from the DLVO theoretical data fits to the HSA probe tip versus $COO^-$-terminated SAM surface experiment, Figure 8). The fit to the theory showed good agreement for $D$ > 4.5 nm with an Au surface charge, $\sigma_{plane}$(Au) = −0.014 C/m$^2$, suggesting that the observed repulsive behavior in this range was electrostatic in origin. It is postulated that these forces might arise, in part, from an effective surface charge on the Au substrate due to nonspecific anion adsorption.[57]

*(D) HSA Probe Tip versus $CH_3$-Terminated SAM Surface.* Figure 10 displays the average $F$ (nN) and $F/R_{tip}$ (mN/m) versus $D$ (nm) approach curves for a HSA probe tip versus a $CH_3$-terminated SAM surface in PBS (blue triangle symbols), as well as the corresponding standard deviations (blue solid lines). A purely attractive, nonlinear interaction curve begins at $D$ < 80 nm, with a jump-to-contact at $D \sim$ 20 nm, a mean attractive minima of $\langle F_{min} \rangle$ = 0.15 ± 0.02 nN, and $\langle F_{min} \rangle / R_{tip}$ = 2.3 ± 0.3 mN/m (this value is a consequence of the cantilever instability, since the slope of the line for $D$ < 20 nm in $dF/dD = k_c$). These data are consistent with previous observations of long-range (∼10−100 nm), attractive forces between hydrophobic surfaces.[58,59] The known van der Waals interaction for a hydrocarbon SAM terminated with a hydrophilic chemical group on Au (eq 2 with $A = 6.92 \times 10^{-20}$J) and the theoretical van der Waals jump-to-contact distance

$$D_{\text{jump-in}} = \left[\frac{AR_{tip}}{3k_c}\right]^{1/3} \qquad (3)$$

which was calculated to be 5.3 nm, are shown in Figure 10 (green line). Here, we see that the measured force is much larger in magnitude and range than that which is known for a hydrocarbon SAM with a hydrophilic end-group on Au. This long-range force is thought to be due to additional attractive interactions between the hydrophobic $CH_3$ end-groups of the SAM and hydrophobic groups on the HSA that take place in aqueous solution. These data provide a supportive, quantitative explanation for why proteins, even extremely hydrophilic ones such as HSA, are observed to readily adsorb to hydrophobic surfaces.[33,60] Some researchers assert that the molecular origin of the hydrophobic interaction is thought to be driven by the entropic penalty (decrease) for rearrangement and ordering of the H-bonded water network into "cages" around dissolved nonpolar substances,[61a] while others assert that it is equally or primarily due to enthalpic Lewis-acid base forces, that is, H-bonding free energy of cohesion of water.[61b] The attractive force was empirically fit to eq 4,[61] as shown in Figure 10 (black line):

$$F(D) = 4\pi R_{tip}\gamma_i \exp\left(\frac{D}{\lambda_0}\right) \qquad (4)$$

where $\gamma_i$ is the surface interfacial energy with water and $\lambda_0$ is the characteristic decay length. The interaction force before the jump-to-contact can be fit well to eq 4 for $\lambda_0$ = 25.6 nm and $4\pi R_{tip}\gamma_i$ = 0.145 nN, yielding $\gamma_i$ = 0.18 mJ·m$^{-2}$.

**Interaction of HSA-Modified Probe Tip with Various Surfaces on Retract.** *(A) General Methodology.* A number of parameters were defined and calculated to characterize the nanoscale adhesion between the HSA probe tip and various surfaces, and they are summarized in Table 2. $F_{adh}$ is the maximum attractive force observed on retraction for each distinct adhesion event (which may occur more than once for a single force curve if multiple molecules of varying lengths are tethered between the tip and the substrate), and $\langle F_{adh} \rangle$ represents the mean value of $F_{adh}$ for one dataset, that is, corresponding to numerous force versus distance curves for one particular probe tip−sample combination (i.e. this notation is used consistently throughout the rest of the paper). $\langle D_{adh} \rangle$ is the mean distance corresponding to $\langle F_{adh} \rangle$. $\langle F_{adh} \rangle / R_{tip}$ is the mean

(57) Biggs, S.; Mulvaney, P.; Zukoski, C. F.; Grieser, F. *J. Am. Chem. Soc.* **1994**, *116*, 9150−9157.
(58) Christenson, H. K.; Claesson, P. M.; Berg, J.; Herder, P. C. *J. Phys. Chem.* **1989**, *93*, 1472.
(59) Feldman, K.; Haehner, G.; Spenser, N. D.; Harder, P.; Grunze, M. *J. Am. Chem. Soc.* **1999**, *121*, 10134−10141.
(60) Petrash, S.; Liebman-Vinson, A.; Foster, M. D.; Lander, L. M.; Brittain, W. J. *Biotechnol. Prog.* **1997**, *13*, 635−639.
(61) Israelachvili, J. N.; Adams, G. E. *Intermolecular and Surface Forces*, 2nd ed.; Academic Press: New York, 1992.

**Table 2**[a]

| | $CH_3$ SAM | $COO^-$ SAM | Au ($n = 46$) |
|---|---|---|---|
| $\langle F_{adh} \rangle$ (nN) | $-1.70 \pm -0.66$ (total $n = 44$)<br>$-1.88 \pm -0.57$ ($n = 37$)[b]<br>$-0.79 \pm -0.19$ ($n = 7$)[c] | $-0.28 \pm -0.38$ (total $n = 119$)<br>$-0.73 \pm -0.27$ ($n = 42$)[d]<br>$-0.15 \pm -0.11$ ($n = 19$)[e]<br>zero adhesion ($n = 58$) | $-1.35 \pm -0.19$ |
| $\langle D_{adh} \rangle$ (nm) | $20.8 \pm 22.5$ (total $n = 44$)<br>$19.2 \pm 16.7$ ($n = 37$)[b]<br>$29.2 \pm 39.8$ ($n = 7$)[c] | $13.5 \pm 48.0$ (total $n = 119$)<br>$0.8 \pm 4.2$ ($n = 42$)[d]<br>$82.6 \pm 95.2$ ($n = 19$)[e]<br>zero adhesion ($n = 58$) | $22.5 \pm 6.3$ |
| $\langle F_{adh} \rangle / R_{tip}$ (mN/m) | $-26 \pm -10$ (total $n = 44$)<br>$-29 \pm -8.8$ ($n = 37$)[b]<br>$-12 \pm -2.9$ ($n = 7$)[c] | $-1.9 \pm -2.5$ (total $n = 119$)<br>$-4.9 \pm -1.8$ ($n = 42$)[d]<br>$-0.98 \pm -0.75$ ($n = 19$)[e]<br>zero adhesion ($n = 58$) | $-21 \pm -2.9$ |
| BCP: | $-6.6 \pm -2.0$[b] | $-1.1 \pm -0.41$[d] | $-4.7 \pm -0.66$ |
| $\langle W_{exp} \rangle$ (mJ/m$^2$) | $-45$ (triangle), $-73$ (ellipse) | $-7.5$ (triangle), $-12$ (ellipse) | $-32$ (triangle), $-52$ (ellipse) |
| $\langle W_{exp} \rangle$/protein ($k_BT$) | | | |
| JKR: | $-6.1 \pm -1.9$[b] | $-1.0 \pm -0.38$[d] | $-4.4 \pm -0.62$ |
| $\langle W_{exp} \rangle$ (mJ/m$^2$) | $-41$ (triangle), $-68$ (ellipse) | $-6.8$ (triangle), $-11$ (ellipse) | $-30$ (triangle), $-49$ (ellipse) |
| $\langle W_{exp} \rangle$/protein ($k_BT$) | | | |
| DMT: | $-4.6 \pm -1.4$[b] | $-1.0 \pm -0.29$[d] | $-3.3 \pm -0.47$ |
| $\langle W_{exp} \rangle$ (mJ/m$^2$) | $-31$ (triangle), $-51$ (ellipse) | $-5.3$ (triangle), $-8.7$ (ellipse) | $-22$ (triangle), $-37$ (ellipse) |
| $\langle W_{exp} \rangle$/protein ($k_BT$) | | | |
| $\langle U_d \rangle$ (J) | $-(7.90 \pm 3.6) \times 10^{-17}$ | | |
| $\langle U_d \rangle$ ($k_BT$) | $-(1.93 \pm 0.88) \times 10^4$ | | |

[a] $n$ = number of data points used in calculation. total = all data including zero adhesion data (if applicable). [b] Surface adhesion without identifiable protein extension, 84% of data (Figure 13a). [c] Identifiable protein extension, 16% of data (Figure 13b and c). [d] Surface adhesion only, 35% of data (Figure 11b). [e] Protein extension, no surface adhesion, 16% of data (Figure 11c).

adhesive force normalized by the probe tip radius, giving an effective adhesive energy of interaction that can be employed universally for all HRFS data employing a hemispherical probe tip. For data conducted with different probe tips, only $\langle F_{adh} \rangle / R_{tip}$ should be compared, not $F_{adh}$, and even then differences may arise due to local variations in probe tip geometry.

For HRFS data exhibiting surface adhesion (as opposed to other long-range adhesive mechanisms), $\langle F_{adh} \rangle$ was converted into an average adhesive interaction energy per unit area, $\langle W_{exp} \rangle$, using adhesion elastic contact mechanics theory, which predicts the pull-off force required to separate a hemispherical tip of radius $R_{tip}$ from a planar surface:

$$\langle W_{exp} \rangle = \frac{\langle F_{adh} \rangle}{\beta \pi R_{tip}} \quad (5)$$

where $\beta = 1.4$ for the Burnham−Colton−Pollack (BCP) theory,[20] $\beta = 1.5$ for the Johnson−Kendall−Roberts (JKR) theory,[21] and $\beta = 2$ for the Derjaguin−Muller−Toporov (DMT) theory.[19] The BCP and DMT theories account for adhesion via surface forces outside the contact area and within the surface interaction area while JKR theory accounts for adhesive forces only within the contact area.[20] For experiments which undergo energy dissipating processes and mechanical hysteresis (nonequivalence of loading and unloading plots), such as the ones presented in this research study, the experimentally measured adhesion energy per unit area, $W_{exp}$, is greater than the ideal, reversible thermodynamic work of adhesion, $W_{adh}$.[62] Although the time scale of characteristic charge relaxation times is very short, that is, of the order of nanoseconds in $H_2O$ at IS = 0.01 M,[63,64] the electrostatic double layer interaction may exhibit hysteresis, when, for example, charged molecules exhibit structural changes on compression which result in a rearrangement of the spatial distribution of the fixed charge groups and do not relax back during the experimental time scale. Surfaces which exhibit attractive interactions such as van der Waals, hydrophobic, and hydrogen bonding are known to sometimes exhibit hysteresis due to an increase in the number of bonds formed and/or structural rearrangement of the surface molecules during the contact time.[53,65]

Apart from employing these parameters to quantify adhesion, the irreversible adhesive energy lost or dissipated during the loading (approach)−unloading (retract) cycle, $U_d$ (J), which is equal to the total area enclosed by the loading and unloading curves (i.e. amount of hysteresis), was calculated as follows:

$$U_d = \int_{D_{max(a)}}^{0} F_{app}(D)\, dD - \int_{0}^{D_{max(r)}} F_{retract}(D)\, dD \quad (6)$$

where $D_{max(a)}$ is the maximum distance of the approach interaction and $D_{max(r)}$ is the maximum distance of the retract interaction. $U_d$ is a measure of the total adhesive energy required to separate the probe tip from the surface, and since the probe tip and surface are much stiffer than the force transducer in these experiments, $U_d$ primarily reflects the dissipative processes taking place at the interface (rather than in the bulk). For force curves which exhibit large surface adhesive forces, the true adhesive interaction profile is hidden within the large regions of cantilever instability, and hence, an accurate value for $U_d$ could not be calculated for such data.

*(B) Interaction of HSA Probe Tip versus $COO^-$-Terminated SAM Surface.* Figure 11 plots typical individual $F$ (nN) and $F/R_{tip}$ (mN/m) versus $D$ (nm) approach and retract curves for an HSA probe tip versus a $COO^-$-terminated SAM surface in PBS solution and shows that three distinct mechanisms of interaction were observed, each described in detail in the following. For the entire

(62) (a) Ghatak, A.; Vorvolakos, K.; She, H.; Malotky, D. L.; Chaudhury, M. K. *J. Phys. Chem. B* **2000** *104*, 4018. (b) van Oss, C. J.; Neumann, A. W.; Absolom, D. R. The Hydrophobic Effect: Essentially a van der Waals Interaction. *Colloid Polym. Sci.* **1980**, *258*, 424−427.

(63) Haus, H. A.; Melcher, J. R. *Electromagnetic Fields and Energy*; Prentice-Hall: Englewood Cliffs, NJ, 1989.

(64) Weiss, T. F. *Cellular Biophysics*; MIT Press: Cambridge, MA, 1995; Vol. 1.

(65) Joyce, S. A.; Thomas, R. N.; Houston, J. E.; Michalske, T. A.; Crooks, R. M. *Phys. Rev. Lett.* **1992**, *68*, 2790.

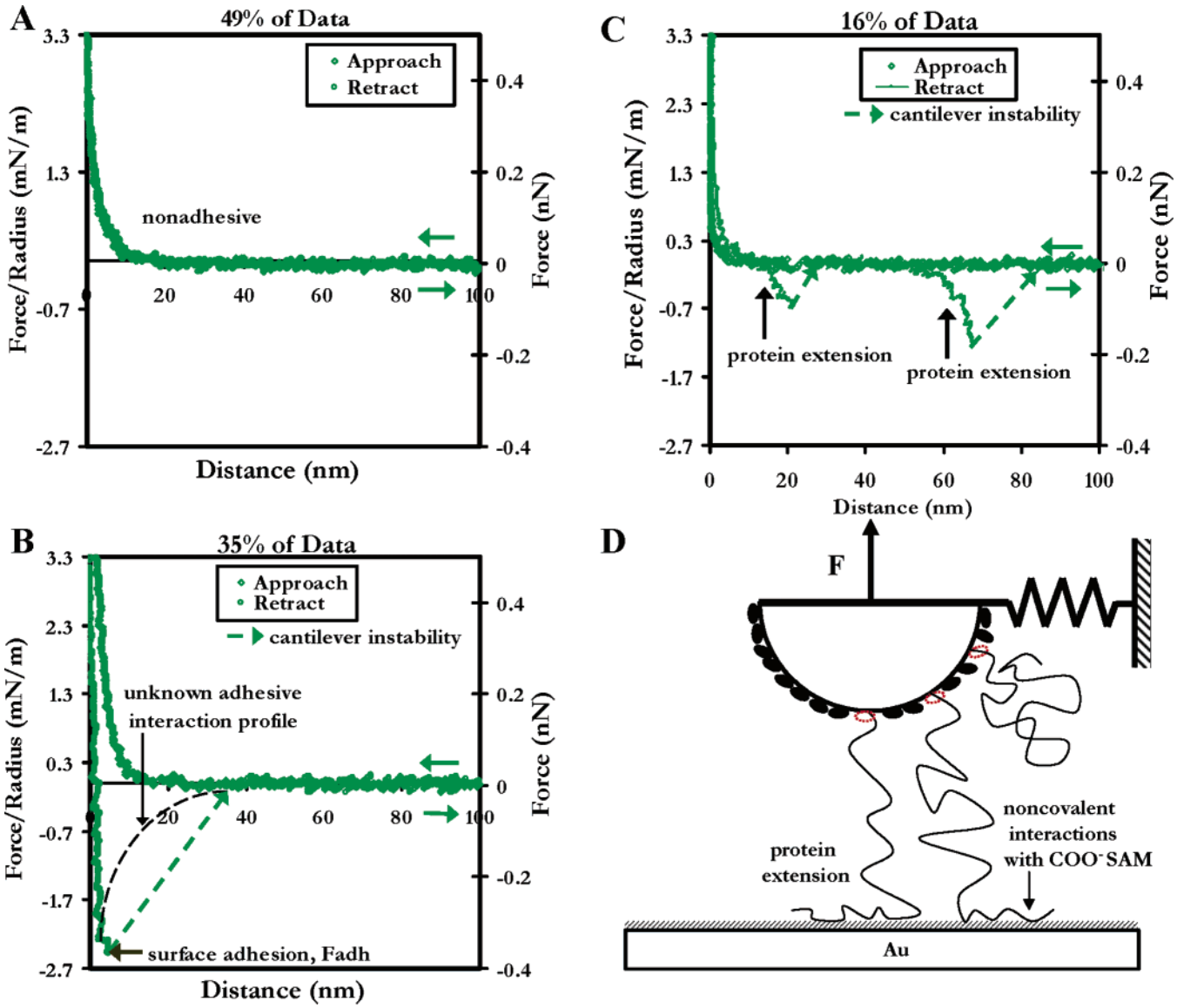


**Figure 11.** Typical individual force (nN) versus distance (nm) approach (green diamonds) and retraction (green circles) curves of an HSA probe tip on a $COO^-$-terminated SAM in PBS ($R_{tip}$ = 65 nm): (A) observed in 49% of the data; (B) observed in 35% of the data; (C) observed in 16% of the data; (D) schematic of proposed adhesive deformation mechanism for the type of force versus distance curve in part C.

dataset, $\langle F_{adh}\rangle(COO^-) = -0.28 \pm -0.38$ nN and $\langle F_{adh}\rangle/R_{tip}(COO^-) = -1.9 \pm -2.5$ mN/m, corresponding to $\langle D_{adh}\rangle(COO^-) = 13.5 \pm 48$ nm.

(1) Completely nonadhesive curves of the type shown in Figure 11A were observed in 49% of the total HRFS experiments where the HSA probe tip exhibited no attractive forces on retraction away from the SAM surface.

(2) Curves of the type shown in Figure 11B (plotted on the same scale as Figure 11A) occurred in 35% of the data. Here, the probe tip exhibited surface adhesion and separated from the surface suddenly at short distances, followed by a region of cantilever instability, where the true adhesive interaction profile was unable to be determined. Hence, $U_d$ was unable to be calculated. For this type of adhesive mechanism, $\langle F_{adh}\rangle(COO^-) = -0.73 \pm -0.27$ nN and $\langle F_{adh}\rangle/R_{tip}(COO^-) = -4.9 \pm -1.8$ mN/m, corresponding to $\langle D_{adh}\rangle(COO^-) = 0.8 \pm 4.2$ nm. $\langle W_{exp}\rangle(COO^-)$ was calculated from eq 5 to be $-1.1 \pm -0.41$ mJ/m$^2$ (BCP), $-1.0 \pm -0.38$ mJ/m$^2$ (JKR), and $-1.0 \pm -0.29$ mJ/m$^2$ (DMT), corresponding to $-5.3$ to $-7.5k_BT$ per protein (assuming triangular shape) and $-8.7$ to $-12k_BT$ per protein (assuming elliptical shape). The contribution to adhesion from the small number of molecules within the elastic contact area versus the larger amount of molecules within the surface interaction area is unknown. A full knowledge of the interaction profile on retract within the cantilever instability region would help clarify this question and could be addressed using stiffer cantilevers with shorter regions of instability (at the cost of lower force resolution). Clearly, the formation and rupture of short-range HSA−SAM noncovalent bonds (this mechanism is further verified by subsequent HRFS data), for example, hydrophobic, van der Waals, hydrogen bonding, are expected to take place mostly within and nearby the elastic contact area, since the surface tethered SAM molecules are too short to access the HSA proteins up the sides of the hemispherical probe tip within the surface interaction area (Figure 16). As mentioned in the Experimental Section, the estimated force per protein at these short distances is much less than the expected force needed for significant structural rearrangements or mechanical denaturation of the proteins. Hence, such short-range SAM interactions are probably most prevalent with accessible surface functional groups of the HSA, for example, with

$NH_3^+$- or OH-functionalized amino acid residues, which remain protonated at pH 7.4. Structural rearrangements of the SAM to facilitate attractive interactions, especially for the few molecules within the elastic contact area, are likely. Such structural rearrangements could also have a significant effect on the long-range attractive forces felt by the surface interaction area. In 12% of force curves exhibiting strong surface adhesion, the region of cantilever instability was followed by protein pulling at longer distances (similar to the curves described in type 3 below).

(3) As shown in Figure 11C (plotted on the same scale as parts 11A and B), in 16% of the data, at short distances there was no surface adhesion, but rather a few long-range, nonlinear attractive peaks were observed where chain segments of the HSA molecules were adsorbed and tethered firmly enough to the SAM surface to allow stretching of the protein molecules between the probe tip and the surface, presumably inducing mechanical denaturation of the HSA. These nonlinear attractive peaks represent the molecular elasticity of a few HSA molecules tethered in parallel between the probe tip and surface (Figure 11D). HSA unfolding can take place at large distances on retract (extension) because there are a smaller number of proteins tethered to the surface, which increases the force per protein, as compared to near the surface when all proteins within the surface interaction area support the applied load in parallel with each other. The multiple regions of cantilever instability may be attributed to mechanical unfolding of a few HSA molecules or different regions of an individual HSA molecule or detachment of individually tethered molecules from the probe tip. It has also been suggested that such experimental data which exhibits force plateaus may be attributed to chains segment "pull-out" from collapsed globules in a poor solvent (i.e. Rayleigh instabilities).[66] The net attractive force, $F_{retract}$, will have contributions from HSA entropic molecular elasticity and enthalpic unfolding forces (deformation and rupture of noncovalent intramolecular bonds) and noncovalent bond deformation and rupture of the HSA chain segments adsorbed to the SAM surface. Presumably, $F_{retract}$ is dependent on the loading rate due to the fundamental kinetics associated with force-driven bond dissociation pathways.[67] For these types of curves, $\langle F_{adh}\rangle(COO^-) = -0.15 \pm -0.11$ nN or $\langle F_{adh}\rangle/R_{tip}(COO^-) = -0.98 \pm -0.75$ mN/m (much less in magnitude compared to previously described surface adhesion mode), corresponding to $\langle D_{adh}\rangle(COO^-) = 82.6 \pm 95.2$ nm (much longer range compared to previously described surface adhesion mode).

*(C) Adhesion of HSA Probe Tip to Au Surface.* Figure 12 plots typical individual $F$ (nN) and $F/R_{tip}$ (mN/m) versus $D$ (nm) approach and retract curves for an HSA probe tip versus an Au surface in PBS solution which was observed in 100% of the total HRFS experiments and appears similar in mechanism to that shown in Figure 11B (observed in 49% of $COO^-$-terminated SAM HRFS experiments). Here, data exhibited large adhesion values and a single pull-off at distances close to the surface that was preceded by a short region in which the force was continuously nonlinear with increasing separation distance. The HSA probe tip exhibited a net attractive force to the Au surface at all separation distances. $\langle F_{adh}\rangle(Au) = -1.35 \pm -0.19$ nN or $\langle F_{adh}\rangle/R_{tip}$ (Au) $= -21 \pm -2.9$ mN/m, corresponding to a distance of $\langle D_{adh}\rangle(Au) = -22.5 \pm -6.3$ nm. $\langle W_{exp}\rangle(Au)$ was calculated from eq 5 to be $-4.7 \pm -0.66$ mJ/m$^2$ (BCP), $-4.4 \pm -0.62$ mJ/m$^2$ (JKR), and $-3.3 \pm -0.47$ mJ/m$^2$ (DMT), corresponding to $-23$ to $-32 k_B T$ per protein (assuming a triangular shape) and $-37$ to $-52 k_B T$ per protein (assuming an elliptical shape). Once again, these curves had large regions of cantilever instability and, hence, the true adhesive interaction profile was unable to be determined.

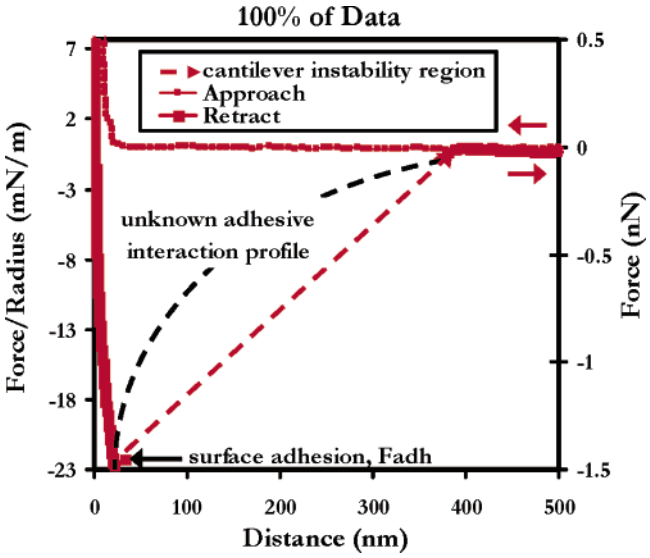


**Figure 12.** Typical individual force (nN) versus distance (nm) approach and retraction curve of an HSA probe tip from Au in PBS ($R_{tip} = 65$ nm).

It has been postulated that the free thiol group on the HSA amino acid residue cysteine-34 may react with the gold surface in these experiments. However, this scenario is in fact rather unlikely, as multiple studies done by electron spin resonance[68,69] and X-ray diffraction studies[36] suggest not only that this residue is buried in a hydrophobic pocket ~9.5 Å beneath the surface of the protein but also that its local environment effectively lowers its $pK_a$ (relative to typical free thiol groups) to 5−8, with values often reported <5. At physiological pH and in our experiments, therefore, Cys-34 is ionized (i.e. in the form of $S^-$ rather than SH) and incapable of reacting with the gold surface.

*(D) Adhesion of HSA Probe Tip to $CH_3$-Terminated SAM Surface.* Figure 13 plots typical individual $F$ (nN) and $F/R_{tip}$ (mN/m) versus $D$ (nm) approach and retract curves for a HSA probe tip versus a $CH_3$-terminated SAM surface in PBS solution and shows two different types of force curves were observed. Curves of the type shown in Figure 13A were observed in 84% of the data, and curves of the type shown in Figure 13B (plotted on the same scale as Figure 13A) occurred in 16% of the total HRFS experiments (for clarity, Figure 13C shows an expanded axis scale of the data given in Figure 13B). For both types of force curves, the HSA probe tip exhibited a net attractive force to the $CH_3$ SAM surface at all separation distances. For the entire dataset, $\langle F_{adh}\rangle(CH_3) = -1.70 \pm -0.66$ nN and $\langle F_{adh}\rangle/R_{tip}(CH_3) = -26 \pm -10$ mN/m, corresponding to $\langle D_{adh}\rangle(CH_3) = 20.8 \pm 22.5$ nm. $\langle W_{exp}\rangle(CH_3)$ was calculated from eq 5 to be $-6.6 \pm -2.0$ mJ/m$^2$ (BCP), $-6.2 \pm -1.9$ mJ/m$^2$ (JKR), and $-4.6 \pm -1.4$ mJ/m$^2$ (DMT), corresponding to $-31$ to $-45 k_B T$ per protein (assuming a triangular shape) and $-51$ to $-73 k_B T$ per protein (assuming an elliptical shape). As shown in Figure 13A, in

(66) Haupt, B. J.; Senden, T. J.; Sevick, E. M. *Langmuir* **2002**, *18*, 2174−2182.
(67) Merkel, R.; Nassoy, P.; Leung, A.; Ritchie, K.; Evans, E. *Nature* **1999**, *397*, 50.
(68) Cornell, C. N.; Chang, R.; Kaplan, L. J. *Arch. Biochem. Biophys.* **1981**, *209*, 1−6.
(69) Graceffa, P. *Arch. Biochem. Biophys.* **1983**, *225*, 802−808.

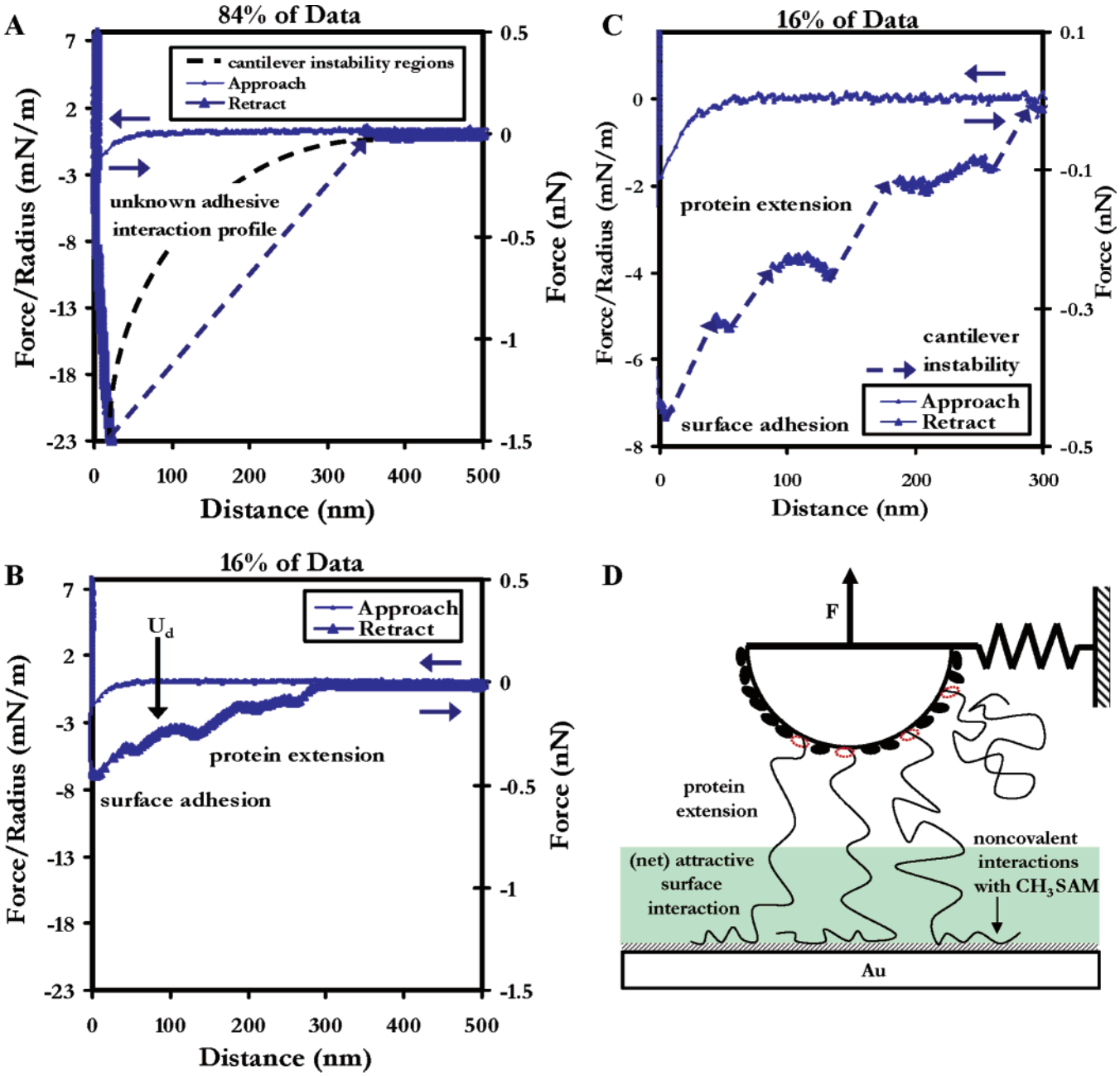


**Figure 13.** Typical individual force (nN) versus distance (nm) approach and retraction curves of an HSA probe tip from a $CH_3$-terminated SAM in PBS ($R_{tip}$ = 65 nm): (A) observed in 84% of the data; (B) observed in 16% of the data; (C) expanded axis plot of part B; (D) schematic of proposed adhesive deformation mechanism.

the HRFS data which exhibited the larger adhesion values, the probe tip separated from the surface suddenly at short distances after a region in which the force grew continuously nonlinear with increasing separation distance. These curves had large regions of cantilever instability, and hence, the true adhesive interaction profile, the range of the interaction, and whether adhesion hysteresis existed (as opposed to mechanical hysteresis of the cantilever) were unable to be determined. As shown in Figure 13B, the force spectroscopy experiments which exhibited smaller adhesion values showed a combination of surface adhesion followed by multiple long-range, nonlinear attractive peaks due to mechanical unfolding of a number of HSA molecules or different regions of the HSA molecules (Figure 13D). More of the force profile is exposed for the HRFS experiments exhibiting smaller adhesive forces (Figure 13B), and a reasonably accurate value for $U_d$ was calculated to be $-(7.9 \pm 3.6) \times 10^{-17}$ J $= -((1.9 \pm 0.9) \times 10^4) k_B T$. The energies per unit interaction area and per protein were unable to be determined, since the interaction area on retract and the number of proteins tethered to the $CH_3$-terminated surface on retract were unknown.

*(E) Statistical Analysis of Adhesion Forces and Distances.* Figure 14A plots $F_{adh}/R_{tip}$ versus $D_{adh}$, and Figure 14B and C compare $\langle F_{adh}\rangle/R_{tip}$ and $\langle D_{adh}\rangle$ for all three surfaces tested, accounting for the entire dataset including all modes of adhesion. The probability distribution histograms corresponding to these data (Figure 14) are shown in Figure 15.

## Summary

In this study, a combined theoretical and experimental approach was employed to study the molecular origins of hemocompatibility of a variety of different model surfaces,

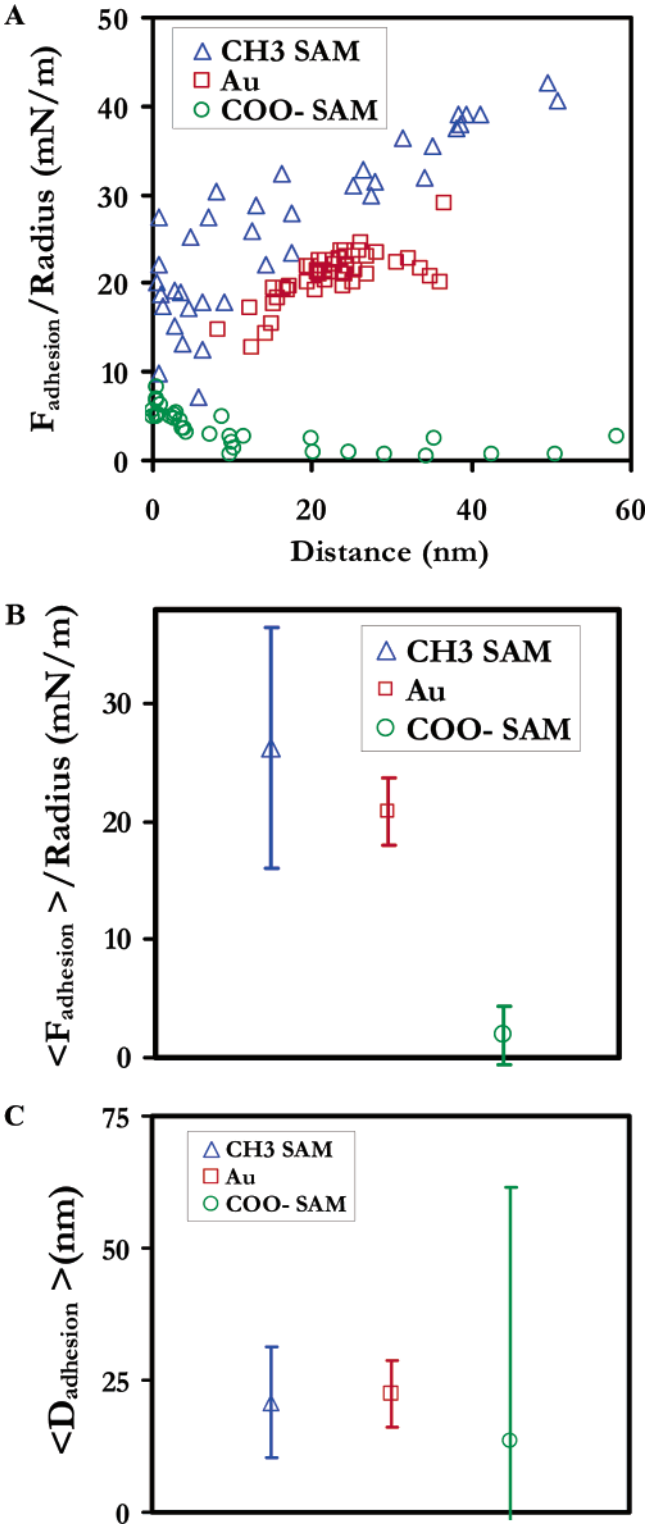


**Figure 14.** (A) $F_{adh}/R_{tip}$ versus $D_{adh}$ for the HSA probe tip on retraction from a $CH_3$-terminated SAM (blue triangles), Au (red squares), and a $COO^-$-terminated SAM (green circles); each datapoint corresponds to one HRFS experiment. (B) $\langle F_{adh}\rangle/R_{tip}$ for the HSA probe tip on retraction from various surfaces. (C) $\langle D_{adh}\rangle$ for the HSA probe tip on retraction from various surfaces.

including Au; a hydrophobic, alkanethiol $CH_3$-terminated SAM; and a hydrophilic, alkanethiol, $COO^-$-terminated SAM. The net force versus separation distance between an HSA-modified probe tip and the surface of interest was recorded on approach and retract in PBS (ionic strength, IS = 0.01 M, pH = 7.4) using the technique of HRFS and compared to quantitative predictions of various theories calculated on the basis of known parameters. Nanoscale intermolecular interactions between alkanethiol SAMs with varying terminal functionality are well-explored in the literature using HRFS; such studies are sometimes referred to as "chemical force spectroscopy".[46,52−54,65,70−80] These experiments have yielded excellent data for testing DLVO theory and producing surface titration curves and information on frictional properties, structural relaxation, surface chemical reactions, and chemically sensitive imaging using AFM. Compared to experiments on SAM−SAM interactions, added complexity probed in our HRFS experiments exists due to the chemical heterogeneity of the protein surface (e.g. charge distribution, hydrophilic−hydrophobic regions, etc.) and the possibility of molecular conformational changes. A few HRFS studies have been reported involving HSA with the atomic force microscope[40,81,82] and the surface forces apparatus (SFA).[37,83]

**HRFS Experimental Data on Approach.** The experimental data on approach were averaged over many experiments and presented always with standard deviations and normalized by $R_{tip}$, giving a representative effective energy of interaction. Calculations of the compressive force per protein on approach within in the maximum surface interaction area are much less than the expected force needed for HSA denaturation, and hence, it is expected that steric deformations of the protein on approach have a negligible contribution to the interaction force profile. The approach interaction of the HSA probe tip on the $COO^-$-terminated SAM and Au substrates was found to be purely repulsive for $D < 15$ nm, nonlinear with decreasing separation distance, and consistent with electrostatic double layer repulsion. A comparison of HRFS experimental data to DLVO theoretical predictions yielded a surface charge per protein of $-1.1e$ to $-1.8e$, depending on the assumed shape of the protein. As expected, these values are less than the known HSA net charge of $-19e$, presumably because many of the charged groups may be unexposed, being located interior to the protein or underneath (facing the probe tip side).

The approach interaction of the HSA probe tip on the $CH_3$-terminated SAM substrate was found to be purely attractive, long-range ($D < 80$ nm), nonlinear with decreasing separation distance, and much greater in magnitude and range than van der Waals interactions between hydrocarbon SAMs terminated with hydrophilic chemical groups on Au. This effect is most likely due to interactions between the hydrophobic $CH_3$ end-groups of

(70) Noy, A.; Vezenov, D.; Lieber, C. *Annu. Rev. Mater. Sci.* **1997**, *27*, 381−421.
(71) Kokkoli, E.; Zukoski, C. F. *Langmuir* **1998**, *14*, 1189.
(72) Kokkoli, E.; Zukoski, C. F. *J. Colloid Interface Sci.* **1999**, *209*, 60.
(73) Kokkoli, E.; Zukoski, C. F. *Langmuir* **2000**, *16*, 6029.
(74) Kokkoli, E.; Zukoski, C. F. *J. Colloid Interface Sci.* **2000**, *230*, 176.
(75) Hu, K.; Bard, A. J. *Langmuir* **1997**, *13*, 5114.
(76) van der Vegte, E. W.; Hadziiouannou, G. *J. Phys. Chem. B* **1997**, *101*, 9563−9569.
(77) van der Vegte, E. W.; Hadziioannou, G. *Langmuir* **1997**, *13*, 4357.
(78) Dufrene, Y. F.; Boland, T.; Schneider, J. W.; Barger, W. R.; U., L. G. *Faraday Discuss.* **1998**, *111*, 79.
(79) McKendry, R.; Theoclitou, M.; Abell, C.; Rayment, T.; Lee, G. U. *Langmuir* **1998**, *14*, 2846.
(80) Werts, M. P. L.; van der Vegte, E. W.; Hadziioannou, G. *Langmuir* **1997**, *13*, 4939−4942.
(81) Kidoaki, S.; Matsuda, T. *Langmuir* **1999**, *15*, 7639.
(82) Kidoaki, S.; Nakayama, Y.; Takehisa, M. *Langmuir* **2001**, *17*, 1080−1087.
(83) Claesson, P. M.; Blomberg, E.; Froberg, J. C.; Nylander, T.; Arnebrant, T. *Adv. Colloid Interface Sci.* **1995**, *57*, 161−227.

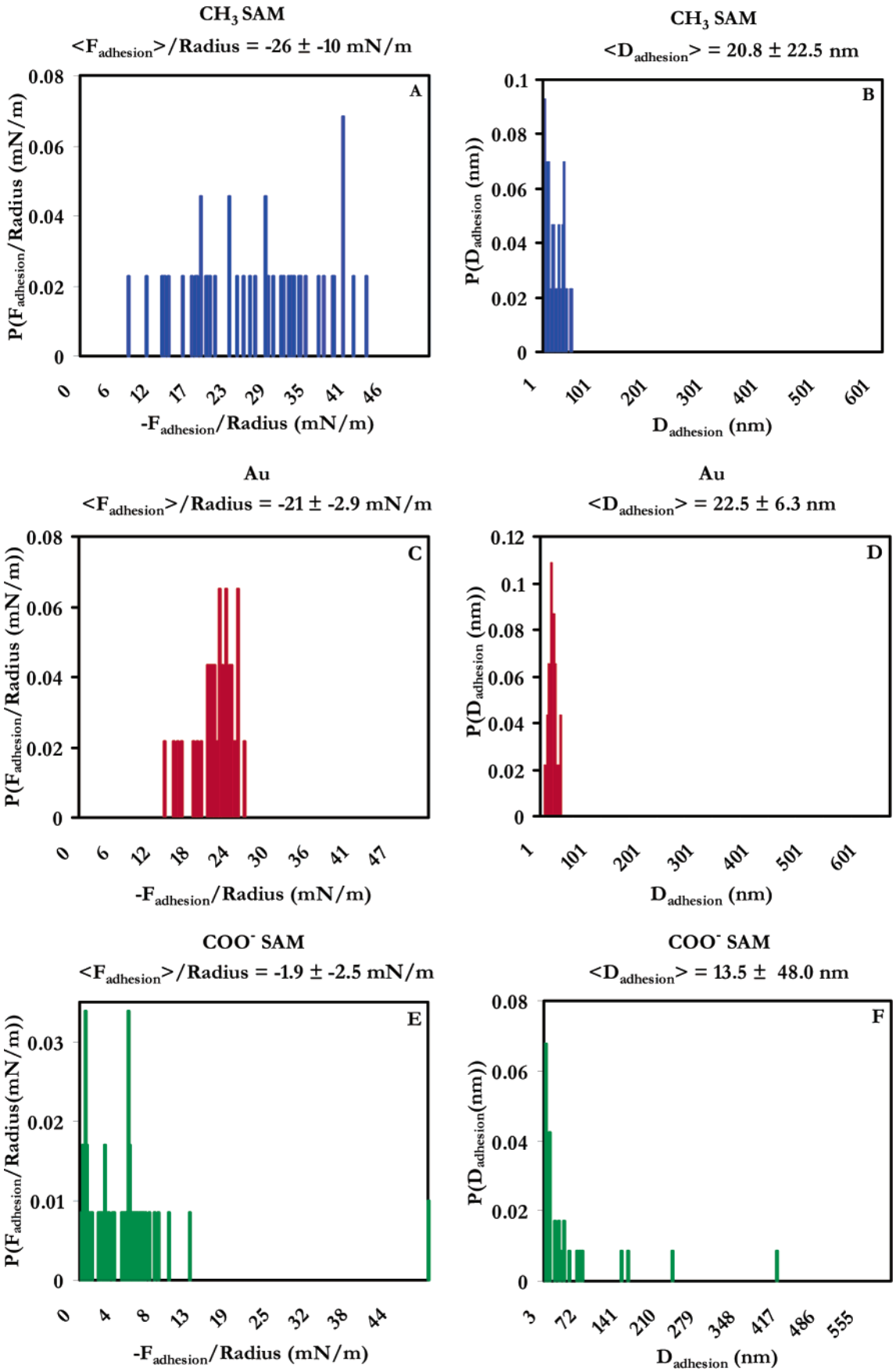


**Figure 15.** Probability distribution histograms corresponding to the experimental data shown in Figure 14: (A and B) $CH_3$-terminated SAM (in blue); (C and D) Au (in red); (E and F) $COO^-$-terminated SAM (in green).

the SAM and hydrophobic groups on the HSA that take place in aqueous solution. The observation of such a strong and long-range attractive force is interesting when one considers that the HSA is complexed with fatty acids which

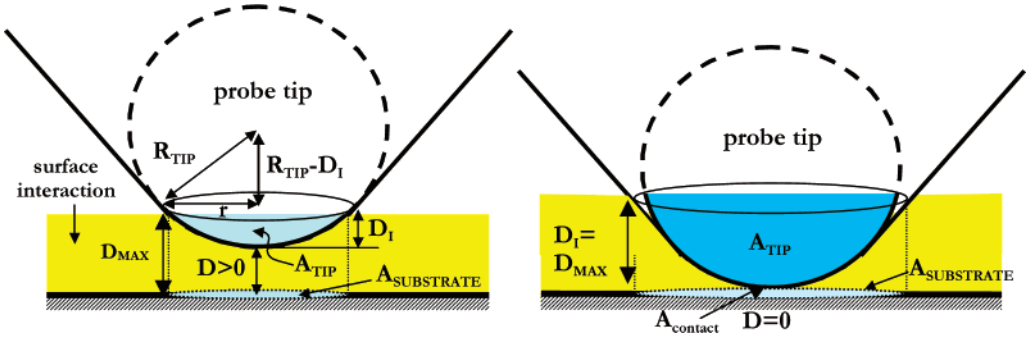


**Figure 16.** Geometry and relevant parameters for defining the surface interaction area between an HSA-grafted probe tip and a surface.

fill up its hydrophobic channels and that the surface of HSA is predominantly hydrophilic. These data provide a supportive, quantitative explanation for why proteins, for example, even extremely hydrophilic ones such as HSA, are observed to readily adsorb to hydrophobic surfaces.[33,60]

**HRFS Experimental Data on Retract.** A number of general parameters were defined to characterize the nanoscale adhesion between the HSA probe tip and various surfaces, that is, $\langle F_{adh}\rangle$, $\langle F_{adh}\rangle/R_{tip}$, $\langle D_{adh}\rangle$, $\langle W_{exp}\rangle$, and $\langle U_d\rangle$, and the validity of each parameter was discussed with regards to the geometry of the HRFS experiment and the type of experimental data obtained. $\langle F_{adh}\rangle/R_{tip}$ is a parameter that can be employed universally for all HRFS data employing a hemispherical probe tip. $\langle W_{exp}\rangle$ was calculated via the JKR, DMT, and BCP elastic contact mechanical theories and can only be employed when the retraction force profile exhibited short-range surface adhesion. $\langle U_d\rangle$ was calculated only in the absence of excessive regions of cantilever instability (typical for weak cantilevers), which prevent knowledge of the true adhesive interaction profile (in the future, stiffer cantilevers with shorter instability ranges will be employed to determine more of the adhesive interaction profile). The adhesion is expected to have contributions from interfacial energy dissipative processes occurring in both the surface interaction area and the elastic contact area, where the forces are amplified over a much smaller length scale (i.e. < 1 HSA protein and <45 SAM molecules are calculated to fit within $A_{contact}$).

Large surface adhesive energies (≤ −29 mN/m, −22 to −73 $k_BT$/protein) were observed for the HSA probe tip on both the $CH_3$-terminated SAM and Au surfaces while smaller surface adhesive energies were observed for the $COO^-$-terminated SAM surface (≤ −4.9 mN/m, −5.3 to −12 $k_BT$/protein). The $COO^-$-terminated SAM exhibited three distinct types of interaction mechanisms, including 49% pure repulsion (nonadhesion), 35% surface adhesion (12% of which also exhibited protein extension after surface adhesion), and 16% protein extension. For the surfaces which exhibited adhesion, it was shown that short-range adhesive contacts between the HSA chain segments and these surfaces give rise to energy dissipating mechanisms, such as HSA entropic molecular elasticity and enthalpic unfolding forces (deformation and rupture of noncovalent intramolecular bonds) and noncovalent bond rupture of the HSA chain segments adsorbed to the surface. $\langle F_{adh}\rangle/R_{tip}$ for the HSA versus $CH_3$-terminated SAM surface is approximately 1 order of magnitude less than that typically observed for interactions between purely hydrophobic surfaces, that is, a $CH_3$-terminated SAM probe tip versus a $CH_3$-terminated SAM surface.[10] Even though the HSA versus Au and $COO^-$-terminated SAM interaction is purely repulsive on approach, significant adhesion was frequently observed on retraction due to interfacial energy dissipating processes that take place during contact. Hence, generally for HRFS adhesion experiments, there is no clear correlation between approaching and retracting profiles without a knowledge of the details of the energy dissipating processes taking place at the molecular level. In fact, the adhesion hysteresis present is a unique signature of those processes and can be employed, in many cases, to characterize them quantitatively.

**Consequences for HSA Adsorption.** It is interesting to note that the systolic blood pressure is typically 120 mmHg = 16 kPa and corresponds to very short separation distances in the HRFS experiments: $D$ = 5.6 nm on approach for the Au substrate (i.e. by calculating the stress = $F/A_{tip}$ from eq A2), $D$ = 4.6 nm on approach for the $COO^-$-terminated SAM, and $D$ = 0 nm for the $CH_3$-terminated SAM (since it only has a purely attractive force). Hence, it is expected that this physiological degree of compression would allow for a high probability of energy dissipating and adhesive mechanisms to occur.

HSA adsorption to SAMs has been observed and studied using total internal refelection fluorescence, neutron reflectivity, and atomic force microscopy (AFM) imaging.[60,84−88] These studies shed light on the conformational changes that take place upon irreversible adsorption, where the area occupied by the protein molecule increases ("spreading"), thus achieving closer contact with the surface until, in many cases, a highly aggregated and entangled, tightly bound network of polypeptide chains results.[89] This process is a balance between the time-dependent formation of noncovalent HSA−surface interactions and structural rearrangement entropic and enthalpic penalties for protein expansion and denaturation. Even though the extensional modes of protein deformation induced in the HRFS experiments on retraction will be different from surface spreading deformations, HRFS can detect and probe the short-range adhesive HSA−surface contacts that are ultimately responsible for both processes, for example by looking at the effect of surface "dwell time" or time delay in contact between approach and retract cycles on the adhesive forces. In the above cited papers, the adsorption process

(84) Choi, E. J.; Foster, M. D. *Langmuir* **2002**, *18*, 557.
(85) Petrash, S.; Cregger, T.; Zhao, B.; Pokidysheva, E.; Foster, M. D.; Brittaini, W. J.; Sevastianov, V.; Majkrzak, C. F. *Langmuir* **2001**, *17*, 7645−7651.
(86) Petrash, S.; Sheller, B.; Dando, W.; Foster, M. D. *Langmuir* **1997**, *13*, 1881.
(87) Sheller, N. D.; Petrash, S.; Foster, M. D. *Langmuir* **1998**, *14*, 4535.
(88) Liebman-Vinson, A.; Lander, L. M.; Foster, M. D.; Brittain, M. J.; Vogler, E. A.; Majkrzak, C. F.; Satija, S. *Langmuir* **1996**, *12*, 2256.
(89) Yang, A.; Galloway, J. A.; Yu, H. *Langmuir* **1999**, *15*, 8405−8411.
(90) Ahimou, F.; Denis, F. A.; Touhami, A.; Dufrene, Y. F. *Langmuir* **2002**, *18*, 9937.

has been shown to be sensitive to the SAM packing density and HSA fatty acid binding, suggesting the importance of SAM chain flexibility and "specific" hydrophobic interactions, that is, SAM alkyl chain penetration into the fatty acid binding sites. Analogous HRFS studies, in addition to the use of "antihydrophobic" agents, such as 2-propanol, will be able to quantify these effects on the intermolecular interactions directly.

## Conclusions

(1) The strength and range of the nanoscale interaction of an HSA-modified probe tip was highly sensitive to the type of alkanethiol SAM terminal functional group.

(2) Although the approach curves for the HSA probe tip versus the $COO^-$-terminated SAM and Au surfaces were purely repulsive on approach due to electrostatic double layer and possibly hydration forces, interfacial energy dissipating mechanisms at the nanoscale lead to adhesion hysteresis on retract. Hence, the experimentally measured adhesive energy per unit area, $\langle W_{exp} \rangle$, is expected to be much greater than the thermodynamic work of adhesion, $\langle W_{adh} \rangle$.

(3) Upon compression, the hydrophilic, alkanethiol $COO^-$-terminated SAM exhibited minimal adhesion to the HSA-modified probe tip ($-4.9$ mN/m, $-5.3$ to $-12 k_B T$/protein) while the hydrophobic $CH_3$-terminated, alkanethiol SAM and Au exhibited significant adhesion hysteresis (more than an order of magnitude greater, $-21$ to $-29$ mN/m, $-22$ to $-73 k_B T$/protein).

(4) Multiple modes of interaction or adhesive mechanisms were observed within a single dataset for the $COO^-$-terminated SAM.

(5) The possible mechanisms involved in HSA adhesion include (a) formation and rupture of short-range HSA−SAM noncovalent bonds, (b) structural rearrangements of the SAM molecules, leading to surface forces hysteresis, and (c) (on retract) entropic and enthalpic penalties for extensional protein denaturation.

**Acknowledgment.** The authors would like to thank Professors Darrel Irvine, Paul Laibinis, and Michael Rubner of MIT for the use of vital surface characterization equipment, Dr. Xueping Jiang and Professor Paula Hammond for the $COO^-$ terminated SAM versus $COO^-$-terminated SAM data, and Mr. J. M. Carter of MIT for supplies and characterization assistance. This research was funded by a National Science Foundation graduate fellowship, a Whitaker Foundation Graduate Fellowship, and the MIT Undergraduate Research Opportunities Program.

## Appendix I. Derivation of Surface Interaction Area between a Probe Tip and Planar Surface

The experimental geometry and schematic of relevant parameters are given in Figure 16. As the probe tip begins to penetrate the interaction distance range (i.e. the distance at which forces just begin to be detected between the probe tip and the surface), the surface interaction area will increase from 0 to a maximum value at $D = 0$. The geometrical parameters are defined as follows: $D$ is the separation distance between probe tip and planar surface, $A_{tip}$ is the effective interaction surface area on the probe tip at $D$, $D_I$ is the distance the probe tip has moved into the interaction range (i.e. $D_I = D_{max} - D$, where $D_{max}$ is the maximum tip−sample separation distance range of interaction), and $R_{tip}$ is the probe tip radius. Using Pythagoreum's theorum, $r$ can be calculated from $R_{tip}$ and $D_I$:

$$r = \sqrt{{R_{tip}}^2 - [R_{tip} - D_I]^2} \tag{A1}$$

The interaction area on the tip is the surface area of a portion of a sphere, which is defined as the following:

$$A_{tip} = \pi R_{tip} D_I \tag{A2}$$

The interaction area on the substrate, $A_{substrate}$, is the projection of the interacting piece of the tip, $A_{tip}$, onto a plane. Therefore, it is just the area of the cross section of the sphere at $D_I$:

$$A_{substrate} = \pi r^2 = \pi({R_{tip}}^2 - [R_{tip} - D_I]^2) \tag{A3}$$

These calculations are summarized in Table 1.

## Appendix II. Calculation of Elastic Contact Area between a Probe Tip and Planar Surface

The elastic contact area, $A_{contact} = \pi a^2$, was calculated from Hertzian elastic mechanics[43] for the substrates displaying no adhesive forces on approach as follows:

$$a = \left(\frac{F R_{tip}}{K}\right)^{1/3}, \quad K = \frac{4}{3}\left(\frac{1 - {\nu_1}^2}{E_1} + \frac{1 - {\nu_2}^2}{E_2}\right)^{-1} \tag{A4}$$

where $a$ = elastic contact area radius, $K$ = reduced elastic modulus, $\nu$ = Poisson's ratio, $E$ = Young's (elastic) modulus, $E_1(Au) = 64$ GPa, $\nu_1(Au) = 0.44$, $E_2(Si_3N_4) = 300$ GPa, and $\nu_2(Si_3N_4) = 0.24$. It was found to be 9.6 nm$^2$ for the $COO^-$-terminated SAM and 5.5 nm$^2$ for the Au surface. $A_{contact}$ was calculated from (modified Hertzian) DMT theory[19] for the $CH_3$-terminated SAM displaying an adhesive jump-to-contact on approach as follows:

$$a = \left(\frac{(F + F_{adh}) R_{tip}}{K}\right)^{1/3} \tag{A5}$$

$A_{contact}$ was found to be 5.7 nm$^2$, which is much less than $A_{substrate}$, $A_{tip}$, and $A_{protein}$. Both of these theories predict nonhysteretic behavior.

## Nomenclature

$a$ = elastic contact radius between probe tip and surface, nm

$A$ = Hamaker constant for van der Waals interaction, J

$A_{contact}$ = elastic contact area between probe tip and surface, nm$^2$

$A_{triangle}$ = area of an HSA molecule, assuming a triangular shape, lying flat, nm$^2$

$A_{ellipse}$ = area of an HSA molecule, assuming an ellipsoidal shape, lying flat, nm$^2$

$A_{SAM\ molecule}$ = surface area occupied by one SAM molecule, nm$^2$

$A_{tip}$ = probe tip surface interaction area, nm$^2$

$A_{substrate}$ = maximum substrate surface interaction area, nm$^2$

$D$ = tip−surface separation distance, nm

$D_{adh}$ = distance at which the maximum attractive force measured on retraction takes place, nm

$D_{jump\text{-}in}$ = separation distance at which the cantilever exhibits an attractive jump to the surface, nm

$D_I$ = distance probe tip has moved in interaction range, nm

$D_{max}$ = maximum tip−sample separation distance range for surface interaction, nm

$D_{max(a)}$ = maximum tip−sample separation distance of the approach interaction, nm

$D_{max(r)}$ = maximum tip−sample separation distance of the retract interaction, nm

$F$ = tip−surface force, nN
$F_{adh}$ = maximum attractive force measured on retraction, nN
$F_{app}$ = force between tip and surface on approach, nN
$F_{electr}$ = intersurface electrical double layer force, nN
$F_{hemis}$ = electrostatic double layer force between charged tip and hemispherical surface (surface charge model), nN
$F_{max}$ = maximum force (either applied on approach or measured as attractive on retract), nN
$F_{min}$ = force of attractive minimum in HSA versus $CH_3$ SAM data, nN
$F_{retract}$ = force between probe tip and surface on retraction, nN
$F_{tot}$ = total DLVO force, nN
$F_{VDW}$ = intersurface van der Waals force, nN
$K$ = reduced modulus for probe tip and surface, Pa
$k_B$ = Boltzmann's constant, $1.38 \times 10^{-23}$ J/K
$k_c$ = cantilever spring constant, N/m
$L_{contour}$(HSA) = contour length of denatured HSA, nm
$n$ = number of force versus distance curves, unitless
$N_A$ = Avogadro's number, $6.022 \times 10^{23}$ $mol^{-1}$
pI = protein isoelectric point, unitless
p$K_a$ = the pH at which the ionizable compound is 50% protonated and 50% deprotonated, unitless
$R$ = radius of sphere in inverse power law for van der Waals force, nm
$R_{tip}$ = probe tip end radius of curvature measured experimentally by SEM, nm
$R_{hemis}$ = radius of hemisphere representing probe tip in surface charge model, nm
$T$ = absolute temperature, K (room temperature = 298)
$U$ = intermolecular potential between protein and surface, J
$U_d$ = energy dissipated during loading/unloading cycle, J
$W_{adh}$ = reversible, thermodynamic work of adhesion energy per unit area, $mJ/m^2$
$W_{exp}$ = experimentally measured adhesion energy per unit area, $mJ/m^2$
$z$ = direction normal to sample surface, unitless

*Greek Symbols*

$\beta$ = prefactor in adhesion contact mechanical theories, unitless
$\Phi$ = electrostatic potential, V
$\gamma_i$ = surface interfacial energy determined from attractive interaction between two hydrophobic surfaces on approach, $mJ/m^2$
$\lambda_0$ = characteristic decay length determined from attractive interaction between two hydrophobic surfaces on approach, nm
$\kappa^{-1}$ = electrical interaction Debye length, nm
$\sigma_{tip}$ = surface charge/unit area on probe tip in electrostatic double layer model, $C/m^2$
$\sigma_{plane}$ = surface charge/unit area on substrate in electrostatic double layer model, $C/m^2$
$\theta_{W(A)}$ = approaching water contact angle, degrees
$\theta_{W(R)}$ = receding water contact angle, degrees
$\Delta\theta_w$ = contact angle hysteresis, degrees

LA026551F